

What controls tropospheric ozone?

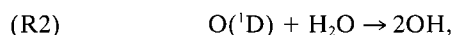
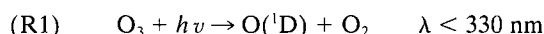
Jos Lelieveld and Frank J. Dentener

Institute for Marine and Atmospheric Research, Utrecht University, Utrecht, Netherlands

Abstract. We have applied a global three-dimensional chemistry-transport model to quantify the photochemistry of tropospheric O₃ and compare the main source categories. We simulated a 15 year period (1979–1993) on the basis of the European Centre for Medium-Range Weather Forecasts meteorological reanalyses and a time-varying emission data set. We calculate that stratosphere-troposphere exchange (STE) strongly contributes to O₃ in regions where the photochemistry is quiescent. Since such regions play a minor role in radiative and chemical processes, we argue that STE-derived O₃ is much less important than is suggested by its column abundance. By distinguishing between photochemical pathways in the model we calculate that tropospheric O₃ in the extratropical Northern Hemisphere is strongly affected by industrial and fossil fuel-related emissions. In the tropics and Southern Hemisphere, natural emissions still play a major role. Our model results indicate a less important role for man-made biomass burning emissions than previous analyses. Further, the results show that tropospheric O₃ trends are strongly influenced by transports of pollution and by meteorological variability. Scenario calculations for the year 2025 suggest that man-made emissions at low northern latitudes, in particular in southern and eastern Asia, will become a very strong tropospheric O₃ source in the next decades. This will influence O₃ levels on a hemispheric scale so that despite pollution regulations in Europe and North America, surface O₃ will continue to grow.

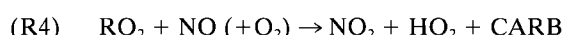
1. Introduction

About 90% of atmospheric ozone is present in the stratosphere, and only 10% is present in the troposphere. Despite this relatively small fraction, tropospheric ozone governs oxidation processes in the Earth's atmosphere through the formation of hydroxyl (OH) radicals. OH, which controls the atmospheric lifetime of many gases, is formed by photodissociation of O₃ in the presence of water vapor [Levy, 1971]:



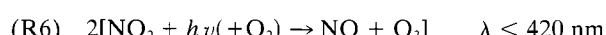
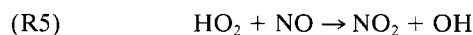
where $h\nu$ is the product of the Planck constant and the frequency of light at wavelength λ .

Traditionally, it was assumed that tropospheric ozone is controlled by stratosphere-troposphere exchange (STE) across the extratropical tropopause [Regener, 1957; Junge, 1962; Danielsen, 1968; Dütsch, 1971]. This first analysis was based on the observed O₃ gradient with altitude, suggesting a source at the tropopause and a sink at the surface. In the 1960s, in situ photochemical ozone formation in the troposphere drew attention as it was shown that the breakdown of hydrocarbons can cause O₃ episodes in urban environments during summer [Haagen-Smit and Fox, 1956; Leighton, 1961]. The in situ O₃ formation is catalyzed by nitrogen oxides (NO_x = NO + NO₂), often emitted simultaneously with hydrocarbons (RH) and carbon monoxide (CO), in particular by man-made sources (Table 1). The main RH oxidation sequence in the atmosphere is

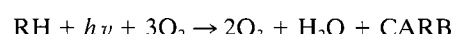


Copyright 2000 by the American Geophysical Union.

Paper number 1999JD901011.
0148-0227/00/1999JD901011\$09.00



Net



Hydroxyl radicals from the reactions (R1)–(R2) initiate the reaction sequence (R3)–(R6) in which O₃ is produced through NO-to-NO₂ conversion and OH is regenerated. Photodissociation of carbonyl compounds (CARB), in particular formaldehyde, yields CO and causes additional ozone formation.

To some extent the above radical reaction chain can be compared with a combustion process for which RH and CO emissions supply the “fuel” [Johnston and Kinnison, 1998]. Some differences, however, need to be emphasized. Combustion itself releases the heat to overcome reaction activation energies, so that spontaneous reactions maintain the process. In the atmosphere solar photons must provide additional energy. At night the sequence ceases. Furthermore, NO_x emissions play a key role. If only the fuel substances RH and CO are added to the tropospheric reaction mixture without NO_x, the HO₂ radicals formed destroy O₃, or they recombine into peroxides. Hence, without NO_x the reaction chain resembles decaying combustion. If this mechanism would prevail in the troposphere, the removal of RH, CO, and other pollutants through OH attack would be fully dependent on O₃ transport from the stratosphere.

In the early 1970s it was suggested that photo-oxidation of the simplest and most abundant of all hydrocarbons, methane (CH₄), and CO can cause O₃ formation in large areas of the troposphere. It was predicted that net tropospheric ozone production predominates in NO_x-rich air, in particular, over much of the continental Northern Hemisphere, while destruction prevails in NO_x-deficient air [Crutzen, 1973]. In subsequent

Table 1. Estimated Annual O₃ Precursor Emissions for the Preindustrial (1860), Recent (1993), and Future (2025) Period

Source Category	CO, TgC yr ⁻¹			NMHC, Tg yr ⁻¹			NO _x , TgN yr ⁻¹		
	1860	1993	2025	1860	1993	2025	1860	1993	2025
Energy use									
fossil fuel combustion	2	112	142	1	37	67	0.3	24.4	41.1
fossil fuel production				0	26	65			
biofuel combustion	22	83	83	8	32	32	0.4	1.3	1.3
aircraft							0	0.5	1.6
Industrial processes	6	15	18	0	56	102	0	1.5	2.8
Biomass burning									
savannah burning	24	77	95	5	15	17	0.9	3.1	3.6
tropical deforestation	8	48	71	1	8	12	0.2	1.1	1.6
temperate wildfires	90	46	50	7	4	4	1.6	0.8	0.9
agricultural waste burning	36	89	156	5	16	19	0.9	2.2	3.9
Agricultural soils							0	2.2	4.5
Natural vegetation/soils	115	115	115	403	403	403	3	3	3
Lightning							5	5	5
NO_y from stratosphere							0.6	0.6	0.6
Natural	205	161	165	410	407	407	10.2	9.4	9.5
Anthropogenic	98	424	565	20	190	314	2.7	36.3	60.4
Total	303	585	730	430	597	721	12.9	45.7	69.9

Here Tg = 10¹² g. Data are from J. A. Van Aardenne et al. (A high-resolution data set of historical anthropogenic trace gas emissions for the period 1890–1990, submitted to *Global Biogeochemical Cycles*, 1999). NMHC is nonmethane hydrocarbons.

years, two lines of thinking evolved about the origin of tropospheric ozone: one emphasized the role of in situ photochemistry [Chameides and Walker, 1976; Crutzen, 1974; Fishman et al., 1979], and the other emphasized that of ozone transport from the stratosphere [Chatfield and Harrison, 1976; Fabian and Pruchnewicz, 1977; Levy et al., 1985].

Recently, three-dimensional (3-D) global chemistry-transport models have been developed to explicitly account for both photochemical and meteorological processes [Crutzen and Zimmermann, 1991; Müller and Brasseur, 1995; Roelofs and Lelieveld, 1995; Berntsen and Isaksen, 1997; Levy et al., 1997; Tie and Hess, 1997; Houweling et al., 1998; Wang et al., 1998; Hauglustaine et al., 1998; Crutzen et al., 1999]. The model results indicate that the mean global tropospheric O₃ column is 350 ± 80 Tg, the transport from the stratosphere accounts for 550 ± 300 Tg yr⁻¹, the net contribution by in situ photochemistry is 150 ± 300 Tg yr⁻¹, and the dry deposition completes the budget through the removal of 700 ± 300 Tg yr⁻¹. The wide ranges of model results illustrate the uncertainties involved. These source and sink terms are suggestive of an important role of STE. However, net in situ photochemistry is the residual of much larger O₃ formation and loss terms, being of order 3000–3500 Tg yr⁻¹. Globally, these terms are in approximate balance. Locally, however, this may be very different, which determines the highly variable O₃ distribution.

The aim of this article is to study the contribution by natural and man-made trace gas emissions to the tropospheric O₃ distribution through photochemistry and to determine the importance of STE. We present results from a global chemistry-transport model that uses European Centre for Medium-Range Weather Forecasts (ECMWF) meteorological reanalysis data to drive tracer transports and removal. Recent model improvements include the representation of STE, nonmethane hydrocarbon (NMHC) chemistry, emissions, and deposition processes. We used 15 years of actual meteorological data and a recently developed historical emission data set to study tropospheric O₃ over the 1979–1993 period and to validate the model by a direct comparison with in situ observations, for example, from ozone sondes. The model is subse-

quently used as a diagnostic tool to quantify O₃ source categories and observed trends. We also present scenario calculations, of historical (1860) and possible future (2025) tropospheric O₃ distributions, the latter based on Intergovernmental Panel on Climate Change (IPCC) recommended moderate growth emission estimates.

2. Model and Emissions

The global transport-chemistry model used has a spatial resolution of 5° longitude and 3.75° latitude. The vertical spacing, in 19 levels up to 10 hPa, is defined according to terrain following sigma coordinates near the surface, pressure coordinates in the stratosphere, and a hybrid of the two in between. Tracer transport, cloud properties, precipitation, temperature, and other physical parameters have been derived from 6-hourly mean meteorological fields from the ECMWF reanalyses over the period 1979–1993 [Gibson et al., 1997]. Tracer advection is simulated with the slopes scheme of Russel and Lerner [1981]. Convective tracer transports are calculated with an updated mass flux scheme that accounts for shallow, midlevel, and deep convection [Tiedtke, 1989]. Turbulent vertical transport is calculated by stability-dependent vertical diffusion [Louis, 1979]. Dry deposition of gases and aerosols is parameterized according to Ganzeveld et al. [1998], and wet deposition is parameterized according to Guelle et al. [1998]. The description of wet deposition accounts for both in-cloud and subcloud removal of gases and aerosols.

A detailed comparison between simulated and measured ²²²Rn indicates that the synoptic-scale model transport properties are represented accurately [Dentener et al., 1999]. Stratospheric O₃ is prescribed above the 10 hPa level, and it is relaxed toward zonal mean O₃ between 10 and 50 hPa on the basis of measurements by the Total Ozone Mapping Spectrometer (TOMS) [McPeters et al., 1996] and ozone sondes [Fortuin and Kelder, 1998], whereas the 3-D ozone variability is maintained by simulated transports. Above 10 hPa a column amount is prescribed on the basis of measurements by the Halogen Occultation Experiment (HALOE) instrument on the

Upper Atmosphere Research Satellite (UARS) [Russell *et al.*, 1993]. Methane is prescribed at the surface on the basis of observations and interpolation with a global model: global mean surface CH₄ for 1860 is 805 ppbv, for 1993 it is 1745 ppbv, and for 2025 it is 2245 ppbv [Etheridge *et al.*, 1998; Lelieveld *et al.*, 1998]. The chemical scheme accounts for 47 species that describe CH₄-CO-NMHC-NO_x-SO_x chemistry of which 32 are transported (including marked tracers). The model accounts for 24 photodissociation, 67 thermal reactions [Houweling *et al.*, 1998], and heterogeneous processes according to Dentener and Crutzen [1993]. The chemistry calculations are performed with a time resolution of 2400 s. Photodissociation frequencies are calculated with the scheme by Landgraf and Crutzen [1998], including the effects of (multiple) scattering by clouds and aerosols and of changing O₃ in the stratosphere [Krol and van Weele, 1997]. The chemical equations are solved with a Eulerian backward iterative solver [Hertel *et al.*, 1993].

Trace gas emission estimates have been recently updated and recalculated on a 1° × 1° grid according to historical information from the Emission Database for Global Atmospheric Research (EDGAR) [Olivier *et al.*, 1996]. Anthropogenic emission calculations have been performed for 10 year intervals since 1860 (J. A. Van Aardenne *et al.*, A high-resolution data set of historical anthropogenic trace gas emissions for the period 1890–1990, submitted to *Global Biogeochemical Cycles*, 1999, hereinafter referred to as Van Aardenne *et al.*, submitted manuscript, 1999). Emission factors account for demographical, economical, agricultural, and technological developments during the past century. Emission estimates for 1860, 1993, and 2025 are presented in Table 1. Note that the 1860, 1993, and 2025 emission scenarios are simulated on the basis of the meteorological data set for 1993. Emission trends of O₃ precursors between 1979 and 1993 are scaled with regional trends of fossil fuel-related CO₂ emissions [Carbon Dioxide Information Analysis Center (CDIAC), 1997].

Biomass burning emission estimates have been improved and evaluated by Marufu *et al.* [2000]. Marufu *et al.* [2000] present a comparison of model results with measurements at low latitudes, mostly over Africa. Natural emissions are distributed according to Lelieveld *et al.* [1998], and those of NMHC are distributed according to Guenter *et al.* [1995]. The anthropogenic emissions have been scaled up to the year 2025 on the basis of the IS92a scenario of the IPCC. This scenario accounts for World Bank and United Nations global population forecasts (2025: 8.4 × 10⁹ people), economic growth (2.3–2.9% yr⁻¹), fossil fuel-related emissions (including an energy use efficiency increase of 0.8–1% yr⁻¹), estimated deforestation rates, and agricultural developments by the Food and Agriculture Organization.

3. Stratosphere-Troposphere Exchange

Stratospheric ozone is formed from O₂ photolysis by short-wave ultraviolet radiation ($\lambda < 240$ nm), mostly in the tropical stratosphere. It is transported poleward in the Brewer-Dobson circulation, which establishes the ozone layer [Brewer, 1949; Dobson, 1956]. The Brewer-Dobson circulation is primarily driven by wave disturbances that originate in the troposphere [Charney and Drazin, 1961; Haynes *et al.*, 1991]. These waves are excited by air flow over mountains, synoptic weather systems, and deep convection. They propagate into the stratosphere where they dissipate, which exerts a drag force onto the

stratospheric westerlies. By thermal wind balance the wave forcing induces poleward motion and a downward mass flux toward the midlatitude and high-latitude troposphere [Holton *et al.*, 1995]. The stratospheric mass balance is maintained by upward motion across the tropical tropopause.

The stratospheric wave propagation is most efficient in the westerly flow during winter [Charney and Drazin, 1961]. Further, orographic wave forcing is strongest in the Northern Hemisphere. Consequently, STE is relatively strongest at mid-latitudes and high latitudes in the Northern Hemispheric winter. Furthermore, seasonal changes in the mass of the lowermost stratosphere also cause STE. During spring the tropopause altitude increases, which entrains stratospheric air into the troposphere [Reiter, 1975; Appenzeller *et al.*, 1996]. The combined effect of these processes is that downward O₃ transport reaches a maximum in late winter and early spring. Since this almost coincides with a spring ozone maximum observed at several background monitoring stations, it is tempting to assume an important role for STE, even at the surface. In section 4, however, we will show that in many locations, especially in the midlatitude Northern Hemisphere, the spring O₃ maximum is due to in situ photochemistry rather than to STE.

In our model we account for STE by constraining zonal and monthly mean stratospheric ozone on the basis of a combination of ozone sonde and satellite measurements [Russell *et al.*, 1993; McPeters *et al.*, 1996; Fortuin and Kelder, 1998]. In the three upper model layers (midlevel at 10, 30, and 50 hPa), column O₃ is relaxed toward zonal mean observations, whereas the 3-D ozone distribution is simulated by ECMWF-based transports. Synoptic waves dominate the extratropical circulation in the troposphere and lowermost stratosphere, being well resolved in the ECMWF-derived air mass transports, and STE is simulated accurately. Plate 1 shows a comparison of modeled O₃ columns with TOMS observations. Note that although the zonal average O₃ density above 50 hPa is prescribed, the longitudinal ozone variability up to 10 hPa is simulated explicitly by the model. This variability results from planetary wave activity, which determines the mean tropopause height. The effects of planetary- and synoptic-scale wave disturbances on O₃ in the lower stratosphere and upper troposphere are thus explicitly accounted for in the model, consistent with the wave forcing of the Brewer-Dobson circulation.

An important indication about the model performance is provided by a comparison of the results with O₃ sonde measurements obtained at midlatitudes and high latitudes between 36° and 74°N, i.e., at Tateno, near Tokyo (Japan), Boulder (central United States), Hohenpeissenberg (Germany), Edmonton (southwestern Canada), and Resolute (northern Canada). Plate 2 shows generally good agreement between model results and measurements, for example, of the seasonal O₃ cycles at both 200 (~12.5 km) and 700 hPa (~3 km). Since 200 hPa is located within the lowermost stratosphere at these latitudes, this indicates that stratospheric ozone, as a boundary condition for our tropospheric ozone simulations, is well captured by the model (Plate 2). Nevertheless, the model does not reproduce some of the highest O₃ peaks at 200 hPa observed when the sondes traverse localized O₃ maxima associated with stratospheric intrusions into the troposphere. These intrusions, or tropopause folds, have a typical dimension of a few tens of kilometers. Because of the horizontal model resolution of 3.75° × 5°, the folds are represented as synoptic-scale features, and cross-tropopause O₃ transport is averaged over a larger area [Kentarchos *et al.*, 1999].

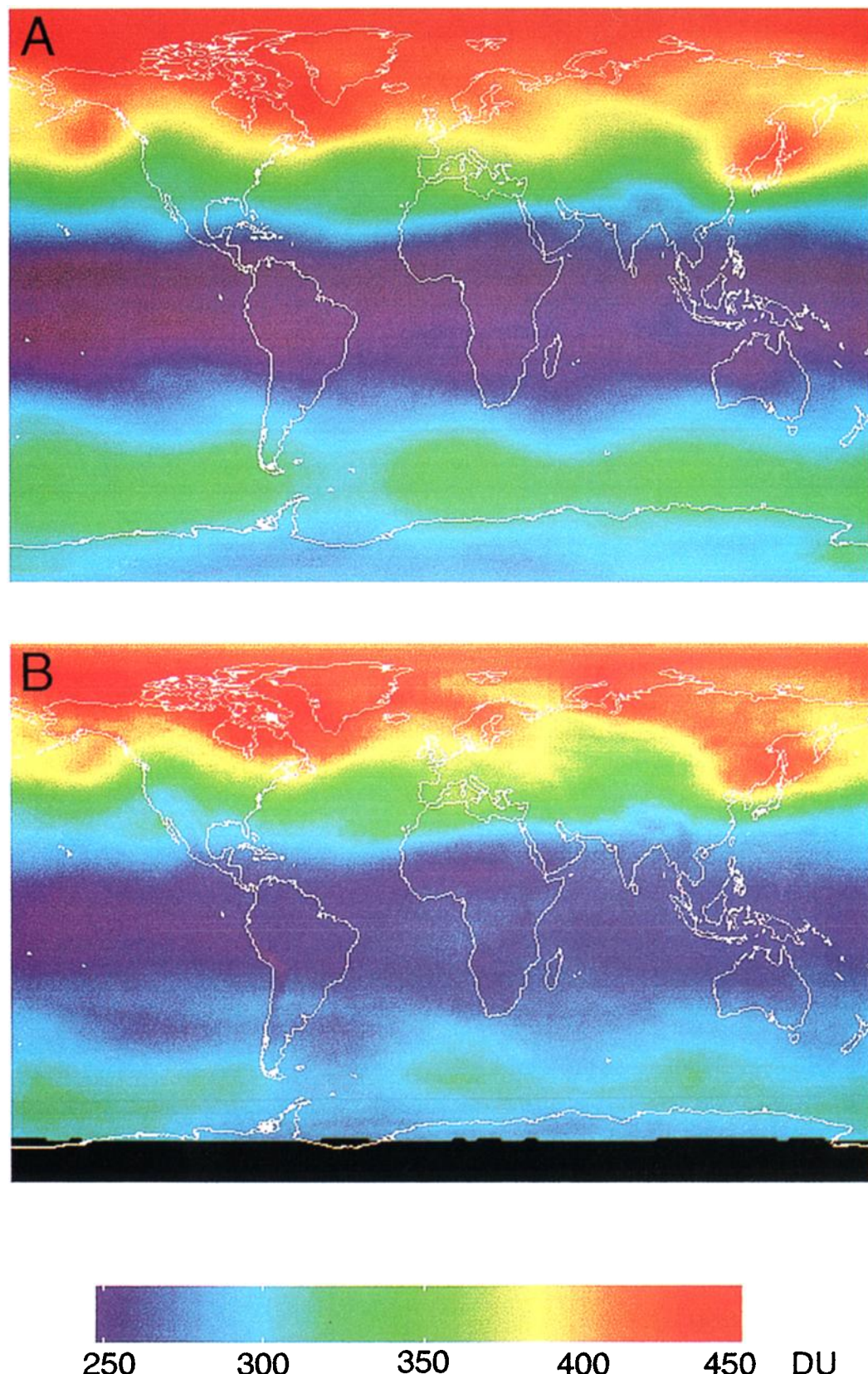


Plate 1. (a) Model-simulated column O₃ compared to measurements by (b) the Total Ozone Mapping Spectrometer (TOMS), both averaged for April 1993, showing that planetary wave-driven variability in total O₃ is well reproduced by the model. The black area indicates an absence of measurements. DU is Dobson Units (1 DU = 2.7×10^{16} molecules cm⁻²).

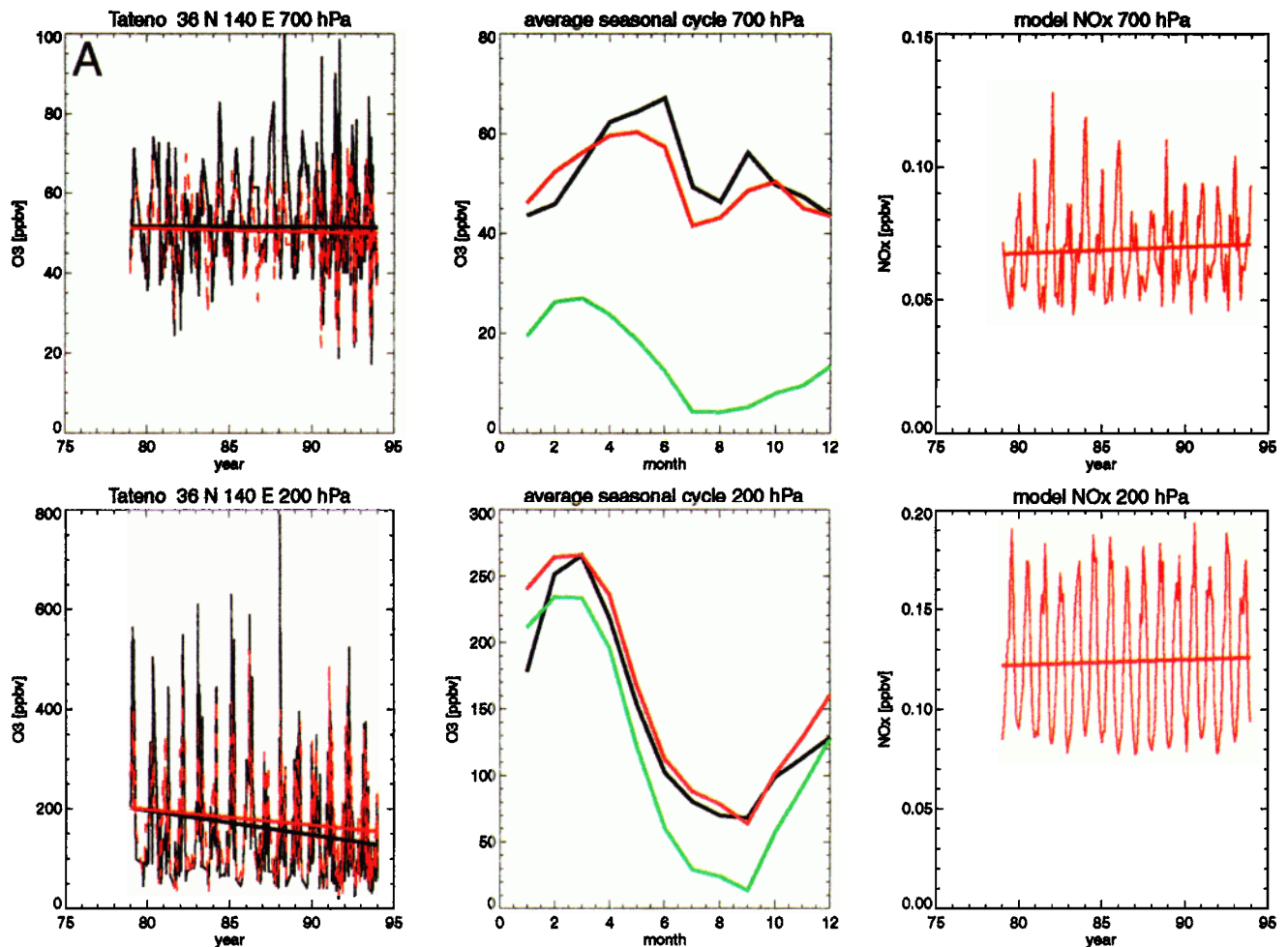


Plate 2. (left) Comparison of model simulations (red) and measurements (black) at (a) Tateno (36°N , 140°E), (b) Boulder (40°N , 105°W), (c) Hohenpeissenberg (47°N , 11°E), (d) Edmonton (53°N , 113°W), and (e) Resolute (74°N , 94°W) on the basis of ozone soundings between 1979 and 1993. The model O_3 has been sampled at about the same times and locations as the sonde measurements. (top) The 700 hPa level and (bottom) the 200 hPa level. Linear trends over this 15 year period are indicated by the straight lines. (middle) The 15 year average seasonal cycles of O_3 . Ozone of stratospheric origin (O_3s) is indicated in green. (right) The model-calculated NO_x mixing ratios and linear trends. The measurement data were obtained from the World Ozone Data Center of the World Meteorological Organization (<http://www.tor.ec.ca>).

Our results indicate that the contribution of STE to the global tropospheric ozone budget is 565 Tg yr^{-1} , in reasonable agreement with the UARS-derived STE flux of $450\text{--}590 \text{ Tg O}_3 \text{ yr}^{-1}$ [Gettelman *et al.*, 1997] and in the middle of the range of recent modeling studies ($400\text{--}850 \text{ Tg O}_3 \text{ yr}^{-1}$) [Lelieveld *et al.*, 1999]. The total model-calculated photochemical O_3 production in the troposphere (3314 Tg yr^{-1}) is in approximate balance with O_3 destruction (3174 Tg yr^{-1}) (Table 2).

4. STE Effect on Surface O_3

The contribution of STE to O_3 levels in the lower troposphere, including its influence on air quality, has been studied for many years [Tuck *et al.*, 1985; Logan, 1985]. In rare occasions, STE events can deeply penetrate the troposphere and reach the surface [Derwent *et al.*, 1978; Davies and Schuepbach, 1994]. Especially, elevated sites can sometimes experience the direct influence of STE [Reiter, 1991; Elbern *et al.*, 1997; Tsutsumi *et al.*, 1998]. In general, however, stratospheric O_3 intrusions associated with extratropical cyclones are followed by

more gradual downward transport through subsidence at the anticyclonic side of these weather systems [Reed, 1955; Danielsen, 1968; Mahlman, 1969]. Our model can only simulate this gradual process since details, such as tropopause folds, occur on a subgrid scale. The favorable comparison of the model results with measurements (Plates 2 and 3) indicates that this limitation is not significant, especially if we focus on timescales of about a week or longer rather than on individual events.

Plate 3 shows the seasonal cycle of O_3 at several monitoring stations as well as the model-derived stratospheric component of surface O_3 (solid green lines). This O_3 fraction from STE has been calculated by adding an O_3 tracer to the model (O_3s) that has the same value as O_3 at the 100 hPa level and above. After transfer across the 100 hPa level, O_3s is destroyed by the same chemical and deposition processes as "regular" O_3 [Follows and Austin, 1992; Roelofs and Lelieveld, 1997]. Chemical loss of O_3 and O_3s is for the most part determined by the reactions (R1) and (R2) and with OH and HO_2 . Reactions that

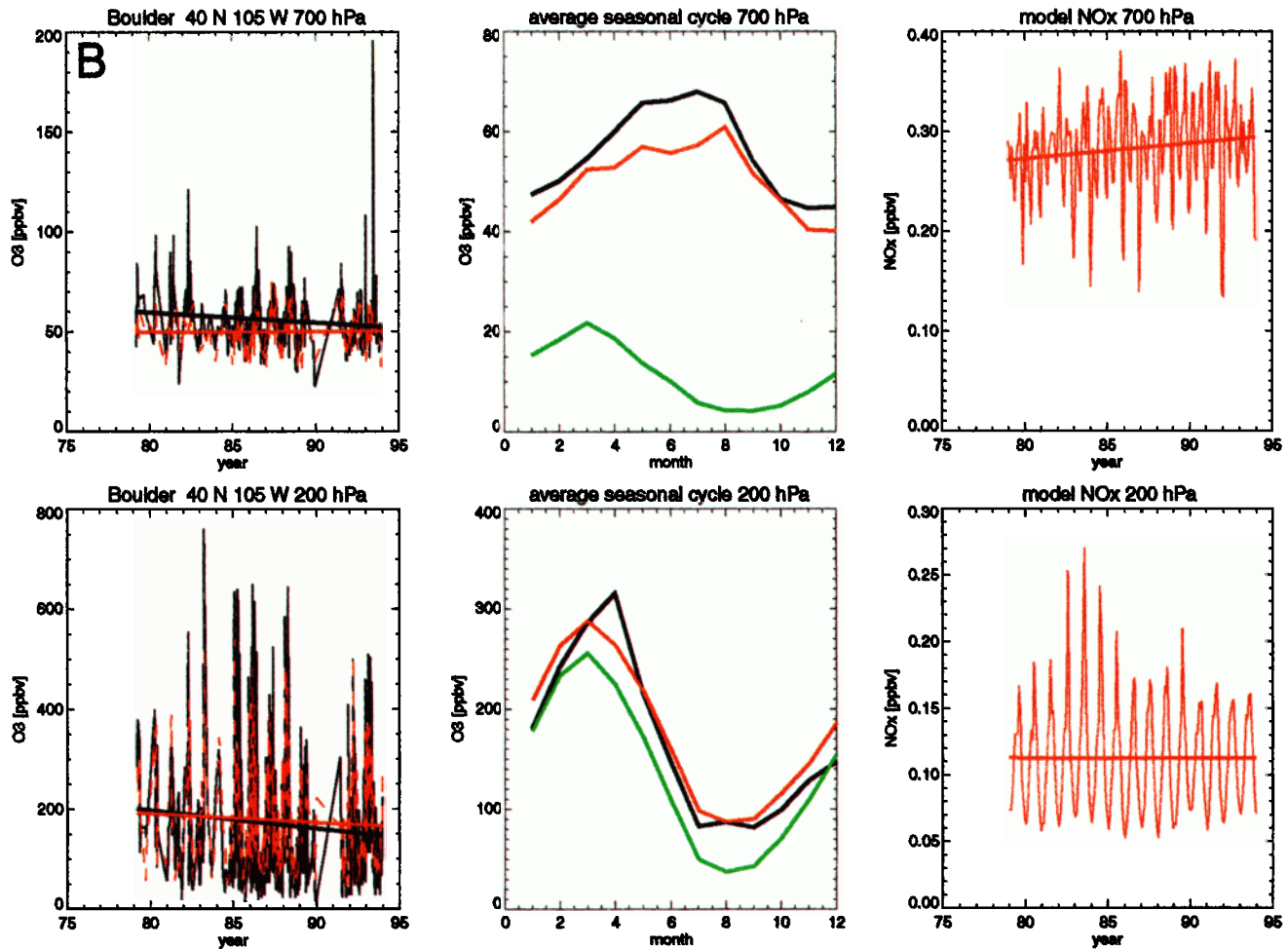


Plate 2. (continued)

do not destroy “odd oxygen” species (e.g., O₃, O, and nitrogen oxides) are not counted as ozone loss. The difference between O₃ and O₃s below 100 hPa equals the amount of ozone photochemically produced within the troposphere (dashed green lines in Plate 3). Interestingly, the column amount of O₃s in the troposphere is hardly affected by temporal changes in tropospheric ozone, for example, by the anthropogenic O₃ increase, as determined from the scenario studies presented in section 7. This implies that the O₃s lifetime is rather constant in time, being largely determined by transport processes. Therefore the “O₃s tracer technique” provides a robust method for estimating the contribution of STE to tropospheric ozone.

Monitoring stations in the extratropical Northern Hemisphere, for example, Jungfraujoch (Switzerland), Mace Head (Ireland), and Mauna Loa (Hawaii), show a clear seasonal O₃ cycle with a maximum during March–May (Plate 3). Note that the Mauna Loa station is located at 3.4 km altitude and Jungfraujoch is located at 3.6 km, i.e., in the free troposphere. As mentioned above, the near coincidence of the spring STE maximum at northern midlatitudes and high latitudes may give rise to misinterpretation. Our model analysis, however, demonstrates that at midlatitudes in the Northern Hemisphere the STE maximum occurs in February–March, at least a month ahead of the seasonal O₃ peak. Plate 3 also shows that during midlatitude spring, photochemical O₃ formation strongly increases. Some pollutants, such as peroxyacetyl nitrate (PAN),

accumulate in the winter midlatitude and high-latitude troposphere because their photochemical removal is slow. After the winter, enhanced breakdown of these gases contributes to O₃ formation [Penkett and Brice, 1986]. In effect, spring conditions (May–June) are optimal for net photochemical O₃ buildup, which more than compensates for the decreasing influence of STE.

As noted in previous analyses [Akimoto *et al.*, 1996; Oltmans *et al.*, 1996; Penkett *et al.*, 1998], pollutant O₃ and its chemical precursors can be transported over long distances from the United States and east Asia, across the North Atlantic and Pacific Oceans, respectively. These transports are quite efficient during winter when photochemical destruction of pollutants is relatively slow. In summer the photochemical lifetime of O₃ in the lower troposphere is only ~2 weeks, and transport is less efficient, so that much photochemically produced O₃ is lost before it reaches, for example, Mace Head and Mauna Loa. In addition, STE has a minimum in summer. Both these effects contribute to the relatively low surface ozone values at these stations during summer. In Tateno at 700 hPa (Plate 2) this summertime O₃ minimum is particularly pronounced because of a sharp STE decline, which gives rise to a double-peaked seasonal cycle.

At Cape Grim, Tasmania, model-calculated surface O₃ is somewhat underestimated during the April–June period (Plate 3). This may be due to an underestimate of long-range trans-

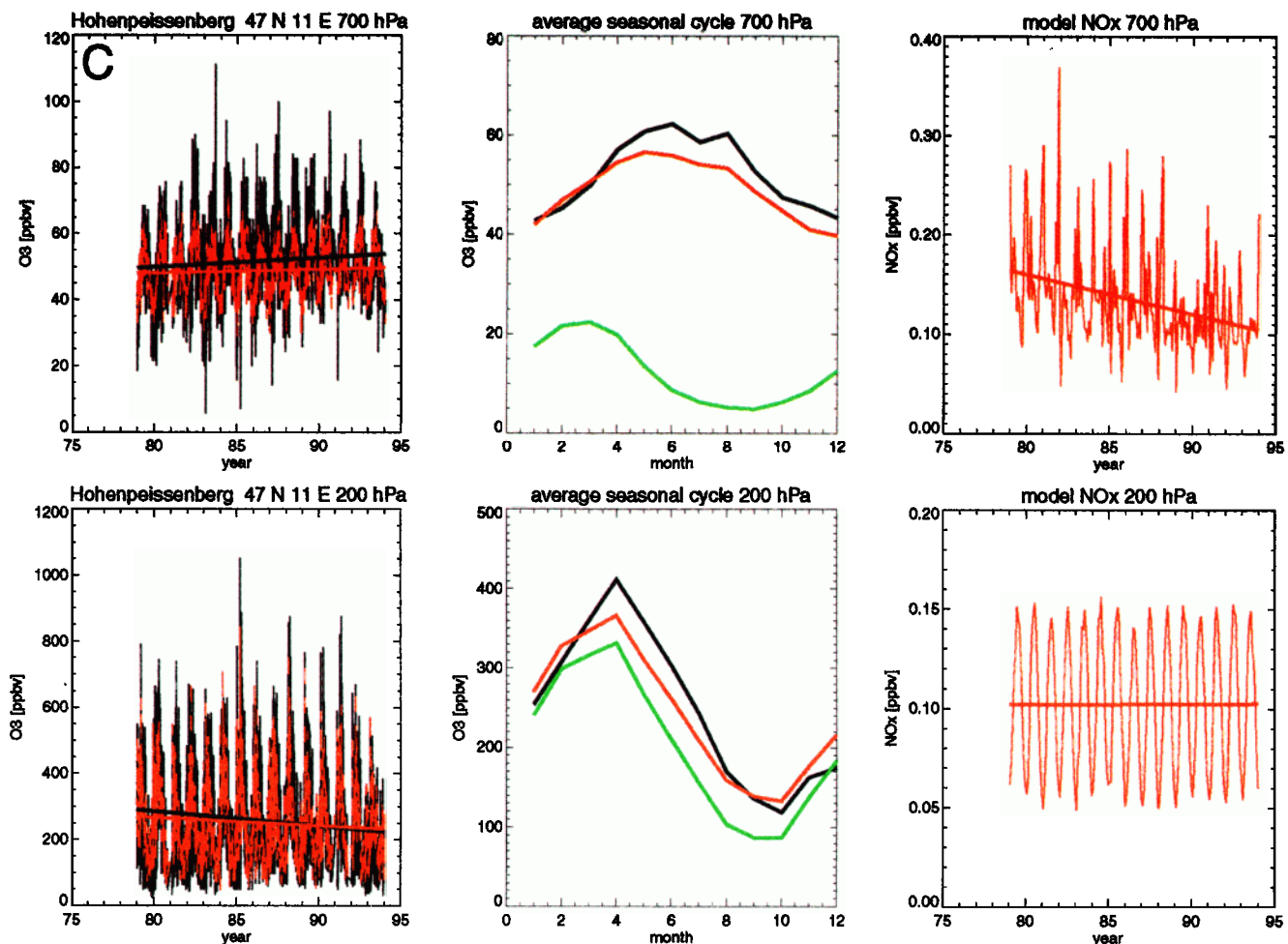


Plate 2. (continued)

ported pollution, for example, from biomass burning in Africa and South America. Our model indicates that the contribution by in situ formed O_3 at this location is fairly constant throughout the year, so that the seasonal cycle is largely determined by STE, which has a maximum in September. Nevertheless, the contribution by in situ photochemistry strongly exceeds that of STE during most of the year. For Cape Point, the southern tip of South Africa, we somewhat overestimate surface O_3 in the biomass burning (dry) season, i.e., in spring (Plate 3). This is caused by artificial dispersion of biomass burning emissions within the large model grid cells ($5^\circ \times 3.75^\circ$). Moreover, O_3 is overestimated in some (1984, 1986, and 1989) but not all years (1983 and 1991–1993), which points to an interannual variability in biomass burning that is not included in our emission database. It is, nevertheless, clear that at this background location, STE contributes significantly less to surface O_3 than in situ photochemistry.

Zonally averaged, in the extratropical Southern Hemisphere the mean STE contribution to surface ozone can reach up to 30–50%. In the extratropical Northern Hemisphere this is <20% in summer and autumn and up to 30–40% in winter and spring, whereas in the tropics it is only ~10–15%. Evidently, transport from the stratosphere contributes most significantly to O_3 in the upper troposphere, where the O_3 lifetime is relatively long because of the low abundance of water vapor and the slow rate of (R2). Furthermore, STE contributes

to tropospheric ozone at midlatitudes and high latitudes in winter when photochemistry is slow and the O_3 lifetime is relatively longest, i.e., at those latitudes and seasons where radiation and oxidation processes are least active.

5. Source Attribution of Tropospheric O_3

To highlight the importance of present-day pollutant ozone, especially during northern summer, Plate 4a shows surface O_3 calculated from a preindustrial emission scenario (Table 1). This picture strongly deviates from that of 1993 (Plate 4b). Late nineteenth century ozone measurements near Paris (at Montsouris) indicate that surface O_3 hardly followed a seasonal cycle, while average O_3 mixing ratios were ~10 ppbv [Volz and Kley, 1988; Volz-Thomas, 1993]. For central and western Europe we calculate an average preindustrial surface O_3 level of ~20 ppbv, which is higher than is indicated by the nineteenth century measurements. Over the continents in the Southern Hemisphere we calculate lower surface O_3 levels, ~10–15 ppbv, which are in better agreement with the available information about preindustrial ozone [Sandroni *et al.*, 1992]. Wang and Jacob [1998] noted the same discrepancy between their model results and the Montsouris data, and they speculated that preindustrial O_3 precursor emissions might be overestimated. However, analyses of Canadian and Greenland ice cores pertaining to the nineteenth century argue against this

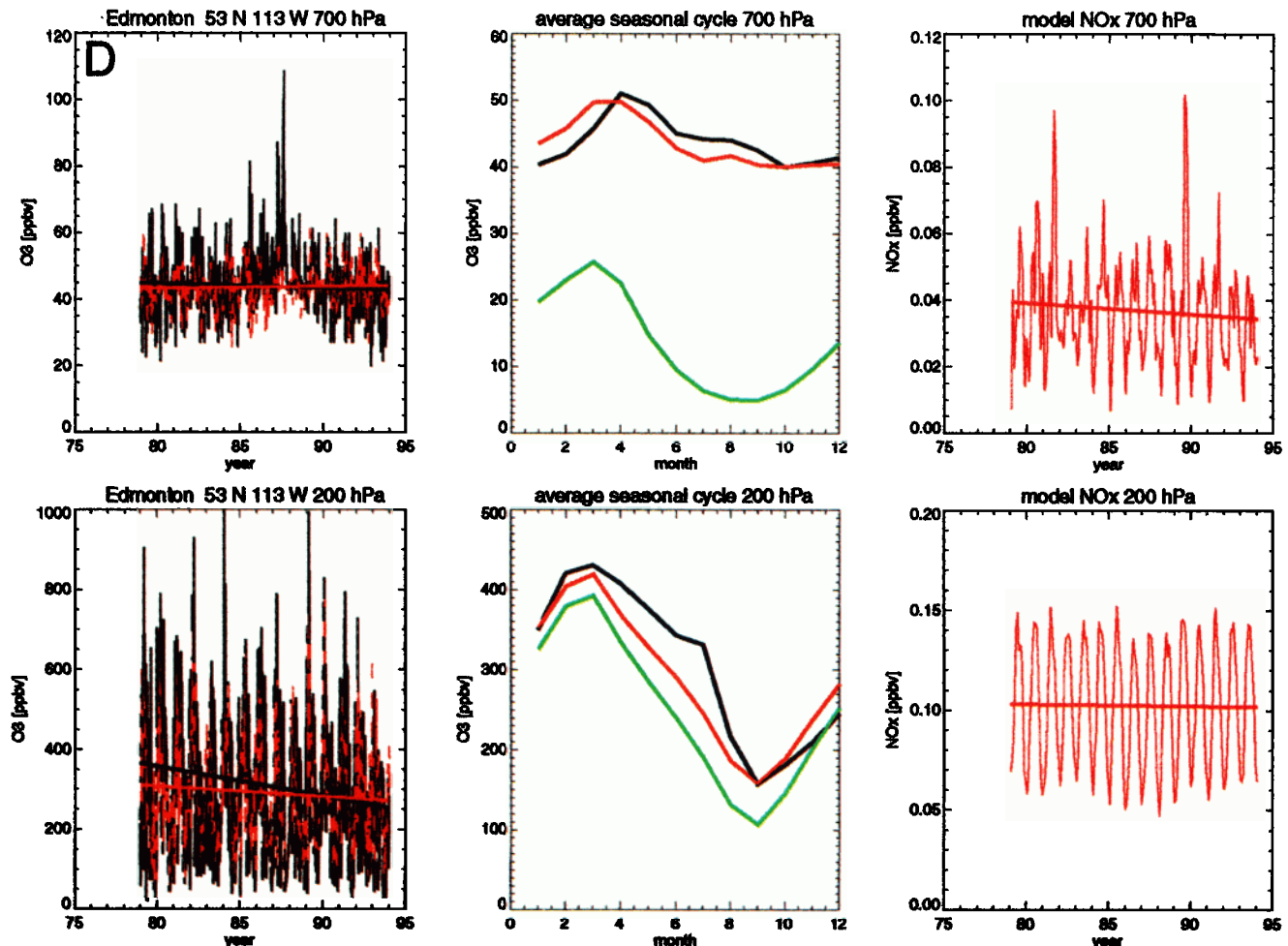


Plate 2. (continued)

possibility as they show clear signals of enhanced biomass burning CO and aerosols [Haan *et al.*, 1996; Holdsworth *et al.*, 1996]. We emphasize that this preindustrial model-data comparison should not be overinterpreted considering the large uncertainty of the reconstructed nineteenth century data, especially of O₃. The fact that we obtain good agreement with O₃ measurements for the present atmosphere (Plates 2 and 3) corroborates that we do not overestimate the man-made contribution to tropospheric O₃.

The model results imply that in the preindustrial troposphere, photochemical O₃ from natural sources contributed about half the surface O₃ in the extratropics, whereas STE contributed the other half. The global mean fraction of stratospheric O₃ within the troposphere (O₃s) was slightly larger than 50% in 1860, 15% more than in 1993, even though the flux of stratospheric O₃ into the troposphere had decreased somewhat in 1993 because of stratospheric O₃ loss (Table 2). Our model produces this STE trend as a result of the (TOMS-derived) O₃ changes in the lower stratosphere. Table 2 also shows that in the preindustrial troposphere, photochemical formation and destruction may have been ~1500 Tg yr⁻¹ less than at present. Hence these terms in the O₃ budget have almost doubled as a consequence of man-made emissions, leading to a tropospheric O₃ column increase of 25%.

Although this 25% increase of tropospheric O₃ is quite substantial, it is less than was previously estimated. Roelofs *et al.*

[1997] and Levy *et al.* [1997] calculated an ~40% increase, and Berntsen *et al.* [1997] calculated a 50–55% increase, whereas Wang and Jacob [1998] and Lelieveld and Van Dorland [1995] obtained an ~65% increase. One reason for the discrepancy is that our preindustrial emission database accounts for some man-made sources, especially from biomass burning (Table 1), whereas previous studies only included natural emissions. Hence we calculate higher surface O₃ levels. Another reason is that the above mentioned models (except Roelofs *et al.* [1997]) distinguish only 7–11 vertical layers, while we apply a 19-layer model. A relatively coarse vertical resolution of the lower troposphere leads to artificial vertical exchange between the boundary layer and the free troposphere [Wang *et al.*, 1998]. This enhances NO_x venting from the boundary layer so that free tropospheric O₃ formation may be overestimated in the models with coarser vertical resolution.

In Plates 5 and 6 we show the calculated contributions to tropospheric O₃ by STE, industrial emissions (including all fossil fuel-related sources), biomass burning, and natural emissions for the preindustrial and present-day atmospheres. The natural emissions include NO_x from lightning and nonagricultural soil exhalation. To distinguish between these sources, we assume that O₃ formation in the troposphere is NO_x-controlled [Crutzen, 1988]. This implies that NO-to-NO₂ conversion by peroxy radicals can be used as a diagnostic for O₃ formation. Moreover, we have labeled tropospheric O₃ that

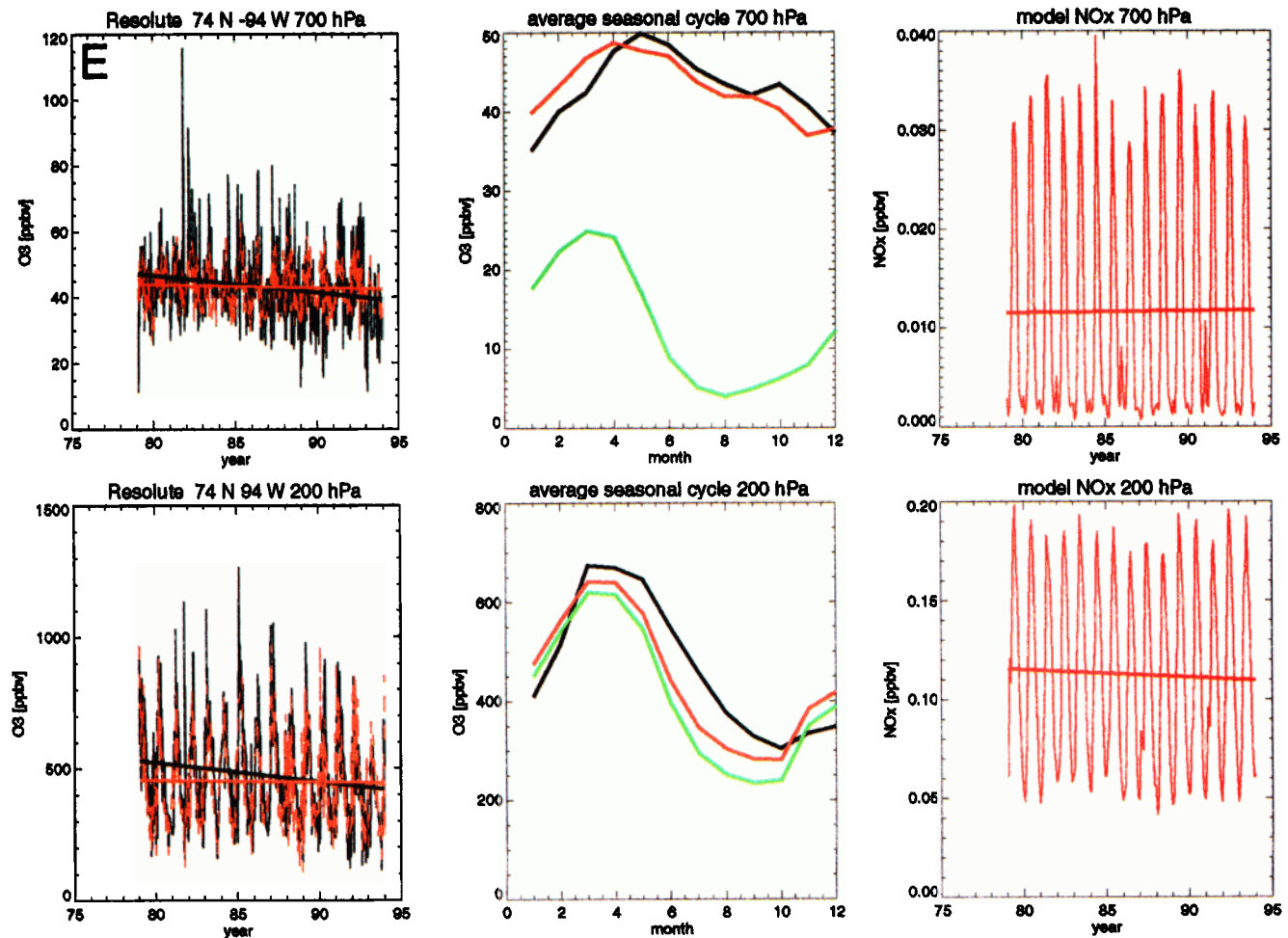


Plate 2. (continued)

has been produced from these NO_x source categories in our model. Note that we also labeled the associated reaction pathways. To check this assumption, we compared the total amount of O₃ formed from these three categories with the calculation of total non-STE ozone in the troposphere (O₃ minus the stratospheric component O₃s). It thus appears that more than

90% of the O₃ produced in the troposphere can be explained by NO_x-controlled photo-oxidation of CO, CH₄, and higher hydrocarbons, in line with regional studies of tropospheric ozone [Sillman *et al.*, 1990; Chameides *et al.*, 1992; Jacob *et al.*, 1993; Pickering *et al.*, 1996]. For consistency the O₃ categories have been scaled to 100%. Furthermore, we have compared the marked tracer approach with simulations in which we switched all emissions on and off per source category [Marufu *et al.*, 2000]. Again, these very different methods yielded very consistent results regarding the sensitivity of O₃ production to precursor emissions.

Plate 5 and Table 3 present the simulated O₃ source attribution for the preindustrial troposphere. Obviously, natural sources prevailed in 1860, although high-latitude biomass burning, associated with forest fires and land clearing, was significant [CDIAC, 1997]. Note that the total amount of biomass burning increased by a factor of 2 between 1860 and 1993 and that the emissions shifted from high to low latitudes. Plate 5 also indicates that O₃s was a significant component of tropospheric O₃, especially at midlatitudes and high latitudes. It appears that photochemical production of O₃ in the 1860 atmosphere was strongly influenced by lightning NO_x; in fact, it was the major global source of in situ photochemical O₃ formation, and it was the dominant overall O₃ source in the tropical troposphere.

From Plate 6 and Table 4 it is quite evident that in 1993,

Table 2. Model-Calculated Global, Annual Tropospheric O₃ Budget for the Preindustrial, Recent, and Future Scenarios

Production/Loss Process	1860	1993	2025
Stratosphere-troposphere exchange, ^a Tg yr ⁻¹	606	565	603
Photochemical formation, Tg yr ⁻¹	1703	3314	4001
Photochemical destruction, Tg yr ⁻¹	1865	3174	3758
Net in situ photochemistry, Tg yr ⁻¹	-162	140	243
Deposition on surface, Tg yr ⁻¹	444	705	846
Tropospheric O ₃ column, Tg	278	347	399
O ₃ s column, ^b Tg	146	131	139
O ₃ t column, ^b Tg	132	216	260

^aThe temporal change in stratosphere-troposphere exchange (STE) results from stratospheric O₃ destruction. For 1860 we adopted the "preozone hole" (1979) conditions; for 2025 we (optimistically) assumed near recovery of the ozone layer.

^bO₃s results from STE, and O₃t results from in situ photochemical formation.

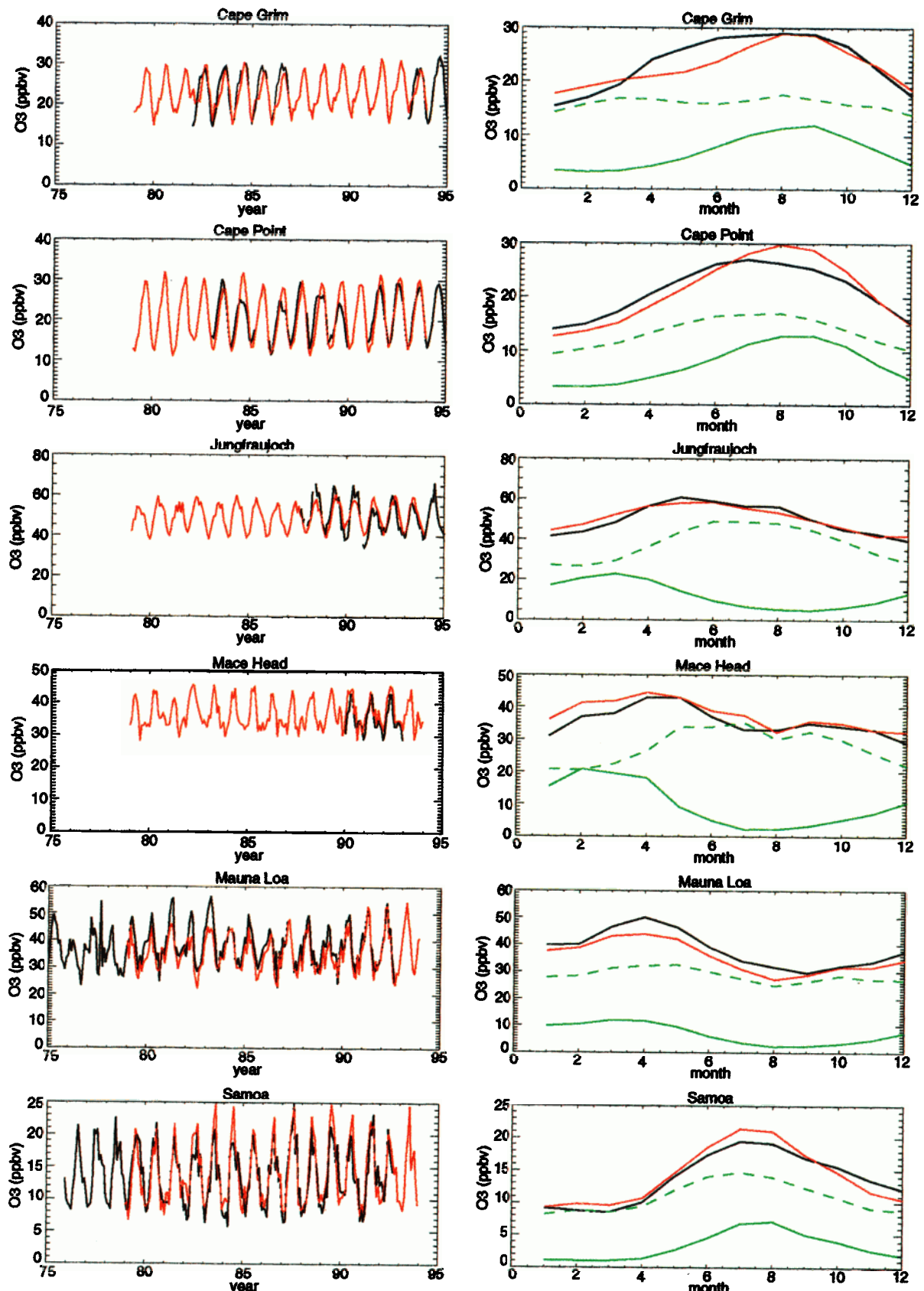


Plate 3. Observed (black) and simulated (red) surface O_3 at several background monitoring sites. Cape Grim (Australia) is located at 41°S, 145°E, Cape Point (South-Africa) is located at 42°S, 18°E, Jungfraujoch (Switzerland) is located at 47°N, 8°E (3.6 km altitude), Mace Head (Ireland) is located at 53°N, 10°W, Mauna Loa (Hawaii) is located at 19°N, 155°W (3.4 km altitude), and the Pacific island Samoa is located at 14°S, 171°W. (right) Average seasonal cycles. Model-calculated ozone of stratospheric origin (O_{3s}) is indicated with the green solid line, and O_3 from in situ tropospheric formation is indicated with the green dashed line. Measurements are by courtesy of the National Oceanic and Atmospheric Administration (NOAA), S. Oltmans, E. Brunke, H. Scheel, and J. Stähelin (<http://www.badc.rl.ac.uk/data/toms/references.html>).

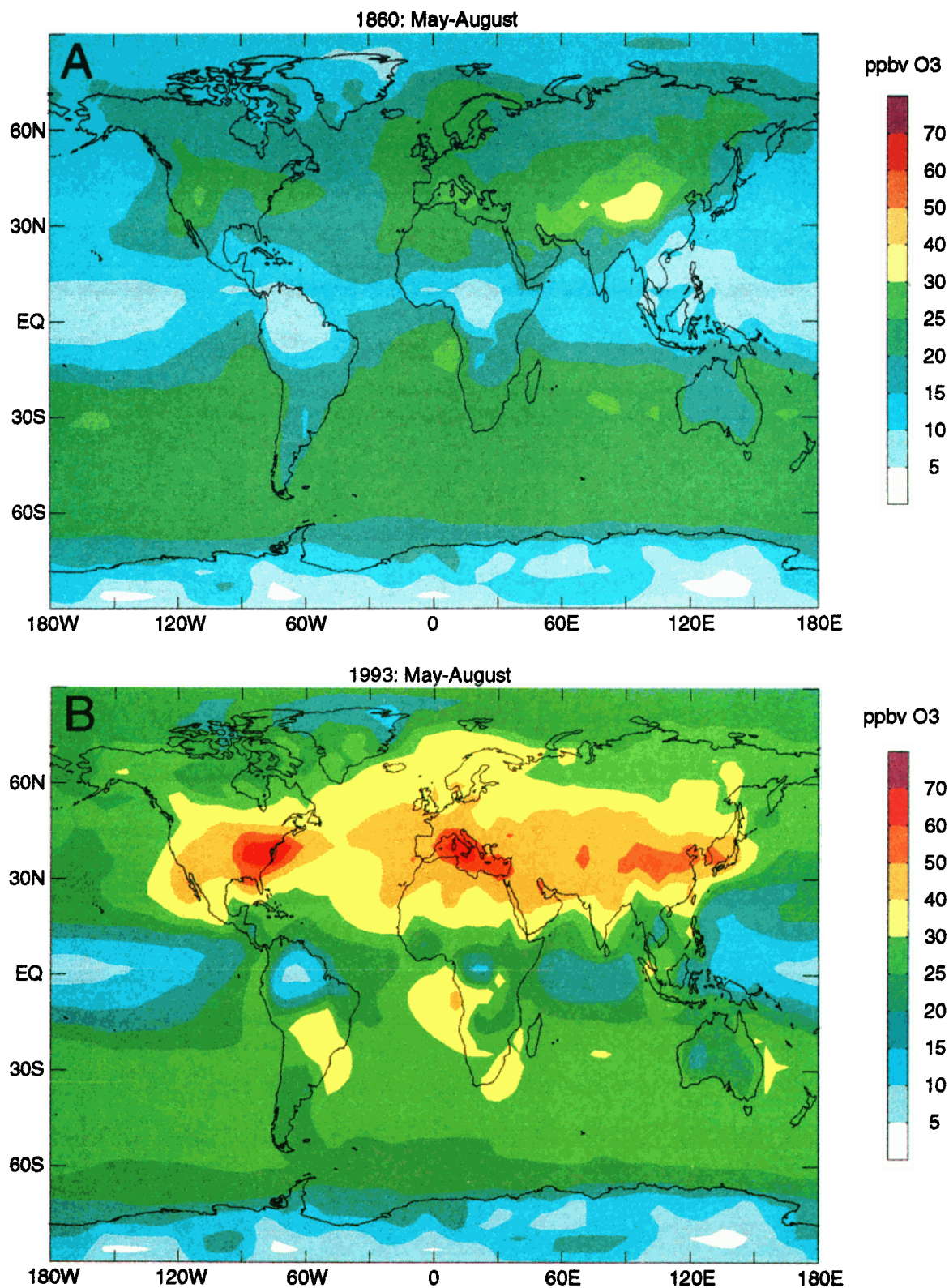


Plate 4. Model-calculated surface O_3 in ppbv during the growing season in the Northern Hemisphere (May–August), comparing the (a) 1860, (b) 1993, and (c) 2025 emission scenarios.

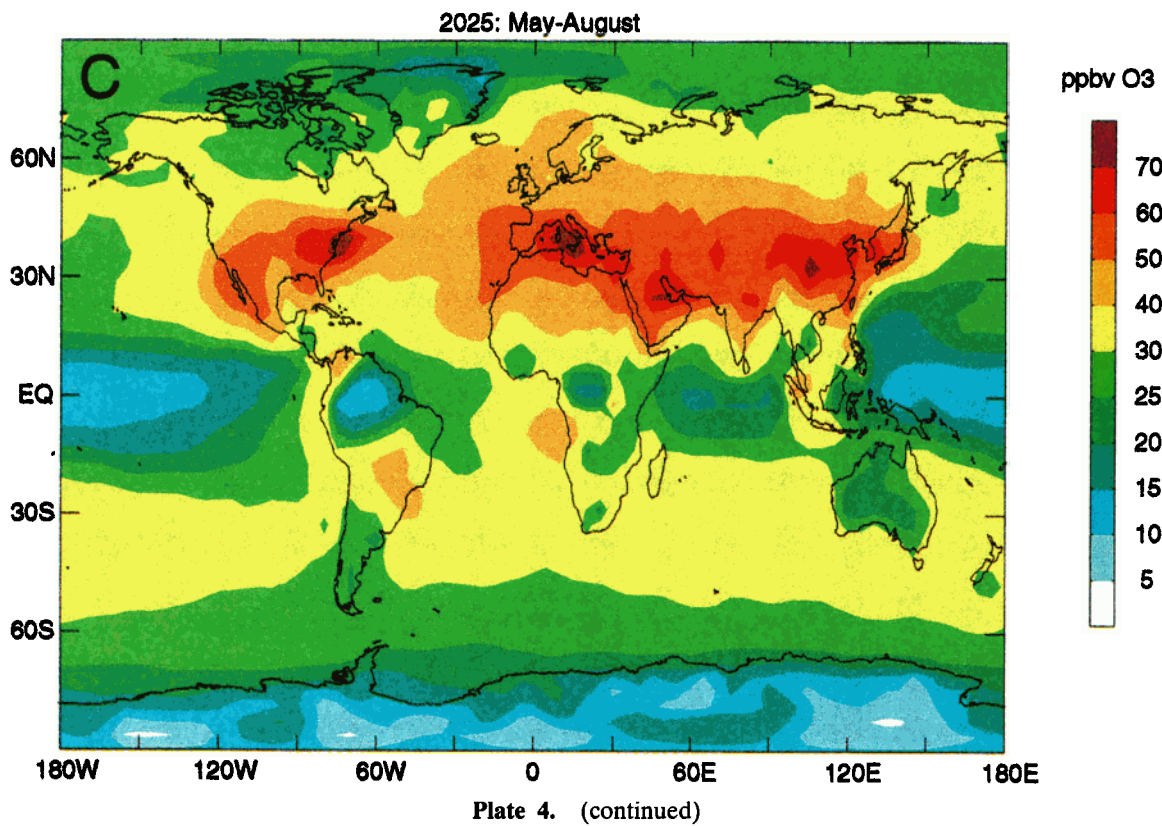


Plate 4. (continued)

fossil fuel-related and other industrial emissions became an important source of tropospheric O_3 , especially in the extratropical Northern Hemisphere. This is not only the case at the surface; more than 40% of the ozone up to ~ 6 km altitude derives from this source category. Despite the fact that STE and natural O_3 formation have changed little since 1860 in our calculations their relative contributions to the tropospheric O_3 budget have declined significantly. The model results illustrate, nevertheless, that natural O_3 precursor sources remain quite important, especially in the tropics, where lightning NO_x -derived ozone prevails. We emphasize, however, that estimates of natural NO_x emissions, both from lightning and soils, are quite uncertain. Soil NO_x emission estimates for the present-day atmosphere range from 5 to 12 Tg N yr^{-1} [Lelieveld *et al.*, 1999]; in our model we apply 5.2 Tg N yr^{-1} for 1993 (Table 1). For lightning NO_x emissions we apply a global source of 5 Tg N yr^{-1} , whereas emissions estimates based on many different methods range from 2 to 20 Tg N yr^{-1} and even much higher, although it seems unlikely that this source exceeds 10 Tg N yr^{-1} [Lelieveld *et al.*, 1999]. Future work will need to reduce these uncertainties.

Plate 6 and Table 4 indicate that biomass burning emissions currently contribute $\sim 10\text{--}15\%$ to the tropospheric ozone column at tropical latitudes, which is less than that of industrial emissions. This may seem relatively small, as previous studies have emphasized the importance of biomass burning [Delany *et al.*, 1985; Fishman *et al.*, 1990; Diab *et al.*, 1996]. However, biomass burning emissions are strongest during the dry season when subsidence suppresses precipitation as well as large-scale dispersion of pollution. The latter is to a large extent dependent on boundary layer venting by deep convection. Thunderstorm convection over land efficiently mixes the troposphere vertically, and importantly, it adds natural NO_x to the burning

effluents [Pickering *et al.*, 1996; Thompson *et al.*, 1996]. In our model, O_3 formation that is catalyzed by NO_x from lightning and nonagricultural soil emissions is designated as "natural," even though the RH and CO emissions may be anthropogenic. Furthermore, much of the O_3 formation in large-scale burning plumes takes place in the free troposphere. NO_x , particularly at low latitudes, has a very short lifetime in the boundary layer (<1 day), so that a large fraction is locally removed as HNO_3 ; it does not survive convective transport to the free troposphere. Hence the free tropospheric O_3 formation from biomass burning is strongly dependent on lightning NO_x . Finally, we mention that the contribution by northern high-latitude burning is significant as well; this was especially the case in the preindustrial atmosphere when wildfires and forest clearing probably played a more important role than today [CDIAC, 1997].

In the Northern Hemisphere tropics, industrial sources presently contribute 20–30% to column O_3 in the troposphere; in the tropical and extratropical Southern Hemisphere this is 10–20% (Plate 6). The larger industrial O_3 component compared to biomass burning at low northern latitudes is a consequence of the relatively strong NO_x production by fossil fuel combustion. Although a significant fraction of these emissions originates from subtropical latitudes, part of the NO_x and the resultant O_3 can be carried toward the tropics by the trade winds. The equatorial region is a convergence zone for surface emissions. Especially in southeastern Asia, pollutant emissions are growing rapidly. Important uncertainties prevail, however. For example, emissions and convective pollution transports to the free troposphere are poorly quantified. It will be quite important to further our understanding of photochemical and dynamical processes in these regions.

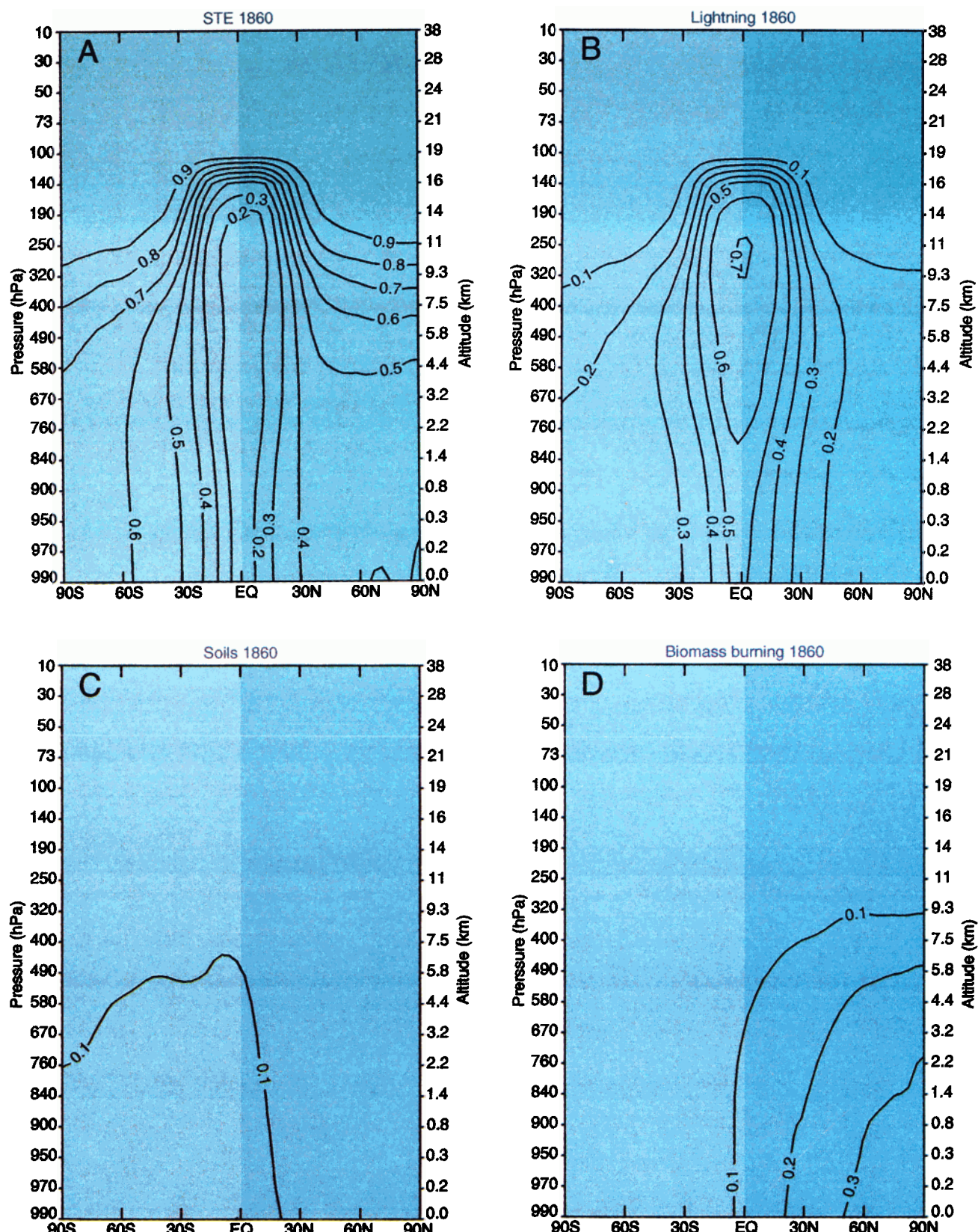


Plate 5. (a) Zonal and annual mean fractional contribution of stratospheric O₃ to total O₃ in the troposphere (STE), the contribution from natural NO_x production by (b) lightning and (c) soil exhalation, and (d) that of biomass burning calculated for the year 1860. The pressure/altitude ordinate shows the mean vertical spacing of the 19 model layers above the surface.

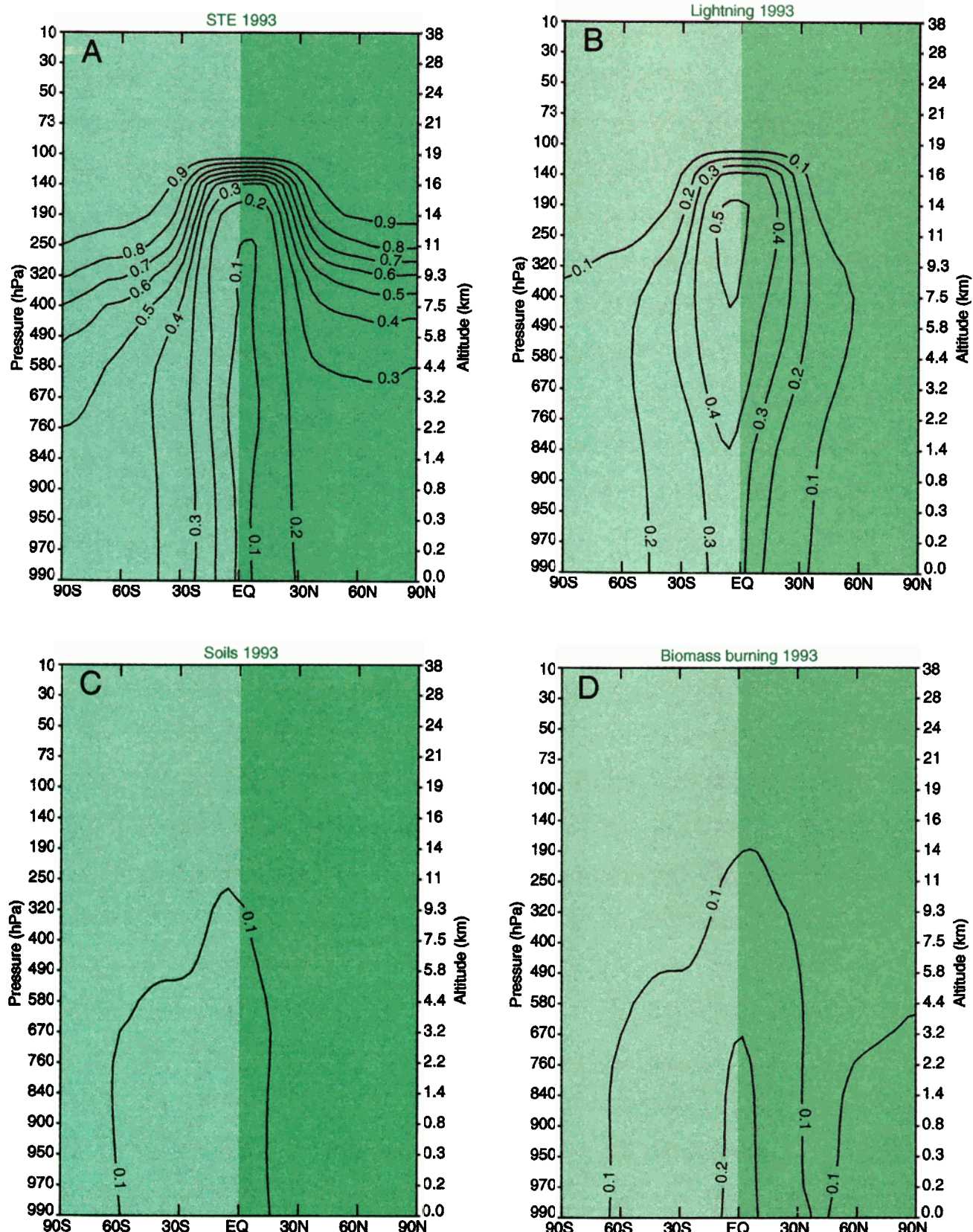


Plate 6. As in Plate 5 but for the year 1993. (e) The contribution by "industry" includes all sources associated with the use of fossil fuels.

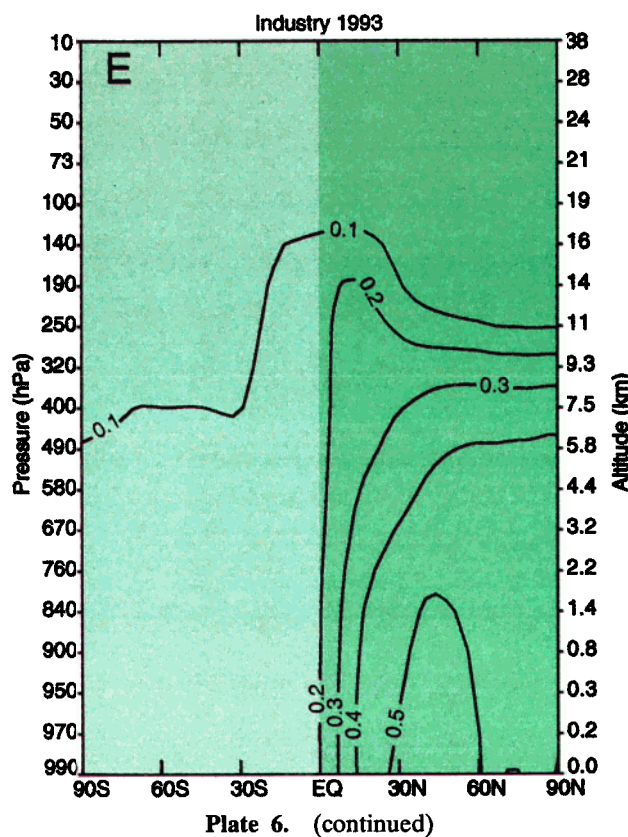


Plate 6. (continued)

6. Calculated Trends

Plate 2 presents calculated and observed O_3 concentrations over the period 1979–1993 obtained at five midlatitude and high northern latitude locations, also showing linear trends at 700 and 200 hPa. In Plates 2a–2e (left) we present O_3 sonde measurements (in black) and the corresponding values from the model (dashed in red) calculated at approximately the same time and location as the sondes. Plates 2a–2e (right) show the model-calculated monthly mean NO_x volume mixing ratios at the same altitude, including the linear trend. Plate 2 illustrates that the seasonal and interannual ozone variability is

substantial. The trend calculations are strongly influenced by the period over which O_3 is measured as well as the sampling frequency. Therefore, in this first analysis we limit ourselves to a qualitative interpretation since it cannot be expected that a global model achieves the high accuracy required to reproduce exactly the observed trends. We merely use the model to indicate which factors might contribute to O_3 trends.

The 200 hPa stratospheric ozone mixing ratios at the five locations in Plate 2 show a negative trend. Clearly, this results from stratospheric O_3 depletion, as observed over the 1979–1993 period [Harris *et al.*, 1995]. Our model systematically underestimates stratospheric O_3 loss and thus the O_3 trend at 200 hPa because it does not account for heterogeneous chlorine activation in the high-latitude lower stratosphere. The calculated negative trend in O_3 largely results from ozone loss above 50 hPa, as derived from TOMS and O_3 sonde measurements being prescribed to the model. The difference between the observed and modeled trend is therefore indicative of O_3 destruction in the lower stratosphere, mostly caused by heterogeneous processes [Fahey *et al.*, 1995; Jones *et al.*, 1995]. The strongest negative trend at 200 hPa occurs during winter and spring. In summer the trend is smallest not only because the influence of stratospheric ozone loss is less significant but also because substantial amounts of tropospheric air penetrate the lowermost stratosphere. Especially in the July–September period, ozone at 200 hPa is strongly diluted by tropospheric air, in particular, over Tateno (Plate 2). The importance of cross-tropopause mixing, especially during summer, has been confirmed by both satellite observations [Appenzeller and Holton, 1997] and aircraft measurements [Lelieveld *et al.*, 1997].

In the troposphere, on the other hand, ozone has increased in many industrialized regions in the Northern Hemisphere. Upward O_3 trends, in particular, during the 1970s, have been derived from ground level and ozone sonde measurements [Janach, 1989; London and Liu, 1992; Logan, 1994; Staehelin *et al.*, 1994; Oltmans *et al.*, 1994, 1998]. In the 1980s, however, these trends declined because air quality control measures started to become effective. In the United States, for example, surface O_3 in rural areas showed very little or no trend over the 1980–1995 period, while in urban metropolitan areas, ozone even decreased [Fiore *et al.*, 1998].

The importance of NO_x in tropospheric ozone photochem-

Table 3. Regional Average Tropospheric Column O_3 and Fractional Contribution Per Source Category for the Year 1860

Region	Area $10^{12} m^2$	Column O_3 , DU	STE, %	Lightning, %	Soils, %	Industry, %	Biomass Burning, %
Canada	13.2	24.8	61	16	6	1	16
United States	12.3	27.4	59	22	6	1	12
Latin America	28.5	21.4	45	42	8	0	5
Africa	35.3	24.3	41	41	8	1	9
OECD Europe	10.8	26.7	61	17	5	2	15
Eastern Europe	14.2	27.5	59	18	5	2	16
Former USSR	25.8	26.5	60	15	6	2	17
Middle East	8.3	27.9	49	33	6	1	11
India region	6.4	25.1	39	41	7	1	12
China region	14.3	24.6	53	28	6	1	12
Southeast Asia	11.0	15.3	30	53	10	0	7
Australia	12.0	28.5	60	29	8	0	3
Japan	1.3	30.9	60	23	5	1	11

DU is Dobson units, United States includes Alaska; Organization for Economic Cooperative Development (OECD) Europe includes Greenland; Southeast Asia is mainly Indonesia and the Philippines; and the Australia region includes the main Pacific islands.

Table 4. As for Table 3 but for the Year 1993

Region	Area 10^{12} m^2	Column O ₃ , DU	STE, %	Lightning, %	Soils, %	Industry, %	Biomass Burning, %
Canada	13.2	32.7	42	9	5	36	8
United States	12.3	37.4	40	13	5	35	7
Latin America	28.5	27.6	33	32	9	16	10
Africa	35.3	33.7	29	28	10	19	14
OECD Europe	10.8	36.1	41	10	5	37	7
Eastern Europe	14.2	38.4	38	10	6	39	7
Former USSR	25.8	35.3	41	9	6	37	7
Middle East	8.3	39.7	33	20	8	30	9
India region	6.4	37.4	25	25	9	27	14
China region	14.3	34.1	36	18	6	30	10
Southeast Asia	11.0	21.9	21	37	9	21	12
Australia	12.0	32.9	49	25	8	10	8
Japan	1.3	42.1	41	14	5	33	7

istry, as indicated above, also applies to trends. *Logan* [1994] noted that in the United States, ozone trends scale approximately linearly with NO_x emissions. Plate 2 shows that at northern midlatitudes, ozone trends are very small at 700 hPa, and this is also the case at the 500 hPa level (the latter not shown). Over Boulder, however, at 700 hPa our model does not reproduce the observed negative O₃ trend. The model indicates that NO_x has increased over the 1979–1993 period at this altitude, which may not be realistic considering that NO_x emissions in the United States were approximately constant in the 1980s up to the mid-1990s [U.S. Environmental Protection Agency (EPA), 1996; *Fiore et al.*, 1998]. It is possible that our emission database overestimates NO_x release from mobile sources in the United States. Although the total volume of traffic has increased, the emission factors have decreased [*Kley et al.*, 1994].

It appears that the calculated NO_x trends at 700 hPa are quite significant at stations that are strongly affected by mid-latitude synoptic weather systems (e.g., Boulder, Hohenpeissenberg, and Edmonton). At these locations we also see a rather strong interannual variability. This applies especially to Hohenpeissenberg, where the calculated NO_x trend at 700 hPa is considerably affected by some episodic high values in the early part of the record and a “depression” of these episodes after 1988. The influence of wind direction is large, and annually varying meteorological conditions strongly affect the NO_x trend.

Detailed inspection of the 700 hPa data presented in Plate 2 reveals that the seasonal cycles of O₃ and NO_x at all stations except Resolute are 6 months out of phase. The highest (episodic) O₃ values occur during summer, while NO_x is highest during winter. This is explained by the relatively long NO_x lifetime during winter and the favorable conditions for photochemical O₃ formation during summer. At Resolute, however, NO_x and O₃ are highly correlated. The total calculated amount of NO_y at Resolute is similar to that in Edmonton; however, NO_x is a factor of 3 lower. We infer that in Resolute, summer-time O₃ buildup results from long-range NO_x transport (notably, NO_y acting as NO_x reservoir), whereas in the other locations, local (grid box-scale) NO_x emissions play an important role.

From the comparison of calculated trends in NO_x and O₃ at 700 hPa, i.e., in the lower free troposphere, an interesting picture emerges (Plate 2). Over Resolute, NO_x was nearly constant during 1979–1993, whereas O₃ slightly decreased. Over Edmonton, NO_x decreased, whereas O₃ hardly changed (despite strong interannual variability). Over Hohenpeissenberg, O₃ slightly increased; however, NO_x substantially de-

creased over the 15 year period. Over Boulder, NO_x somewhat increased, whereas mean O₃ did not change. Over Tateno, NO_x increased, and O₃ was nearly constant. First, it needs to be emphasized that observed as well as calculated O₃ trends were very small at these five locations. Nevertheless, it appears that O₃ trends at 700 hPa do not show a direct relationship with local (grid box-scale) NO_x trends, contrary to the seasonal cycles of these species. Our marked tracer analysis indicates that 65–90% of the NO_x at these locations (at 700 hPa) derives from fossil fuel-related and industrial emissions. The mean NO_x lifetime in the lower free troposphere is several days while that of O₃ is a factor of 10 longer. Therefore, although NO_x is mostly determined by local man-made sources, the trend in O₃ is strongly affected by transport. As will be shown in section 7, this may have important implications for future O₃ trends, which may become positive again, even in the United States and Europe. It should furthermore be stressed that surface O₃ trends in urban areas cannot be explained by NO_x emissions alone because other factors, in particular, NMHC emissions, play an important role as well [*Sillman et al.*, 1990; *Kley et al.*, 1994; *Fiore et al.*, 1998].

Since ozone is a strong oxidant, enhanced levels cause adverse health effects to humans and damage agricultural crops and natural ecosystems [National Research Council, 1991; *Alexis et al.*, 1994; *Chameides et al.*, 1994]. For agricultural crops the cumulative exposure threshold is defined at 40 ppbv over the growing season [*4mann et al.*, 1995]. Plate 4b shows the areas where model-calculated average O₃ levels exceed 40 ppbv at the surface during the months May–August under the 1993 scenario. It appears that the damage threshold is exceeded over most of the Northern Hemisphere continents up to ~50°N. Moreover, average surface O₃ levels in large parts of the United States, the Mediterranean region, and in eastern Asia exceed 50 ppbv, and in some areas even 60 ppbv. Comparison with our pre-industrial scenario calculation confirms that the ozone damage threshold is exceeded solely owing to anthropogenic O₃ precursor emissions.

7. Future Scenario

Although in many western industrialized countries air quality is under legislation, surface O₃ continues to exceed critical levels. In fact, very substantial emission reductions, especially of NO_x, are needed to achieve significant effects [*Chameides et al.*, 1992; *Jacob et al.*, 1993]. Moreover, in southeastern Asia, parts of Africa, and South and middle America, many coun-

Table 5. As in Tables 3 and 4 but for the Year 2025

Region	Area 10^{12} m^2	Column O ₃ , DU	STE, %	Lightning, %	Soils, %	Industry, %	Biomass Burning, %
Canada	13.2	36.5	39	8	6	40	7
United States	12.3	42.3	37	11	6	40	6
Latin America	28.5	32.9	31	26	8	25	10
Africa	35.3	39.9	27	22	11	28	12
OECD Europe	10.8	40.5	38	8	6	41	7
Eastern Europe	14.2	43.6	36	8	6	43	7
Former USSR	25.8	39.7	38	7	7	41	7
Middle East	8.3	47.6	30	16	7	39	8
India region	6.4	45.3	24	19	8	37	12
China region	14.3	39.9	33	14	7	38	8
Southeast Asia	11.0	25.7	20	31	8	30	11
Australia	12.0	37.4	47	22	8	16	7
Japan	1.3	48.5	37	11	6	40	6

tries are developing rapidly, and associated growth of pollutant emissions is inevitable. Since many developing countries are located in the tropics or subtropics, the relatively high UV intensities will boost photochemical pollution.

Plate 4c shows a model prediction of the growing season (May–August) mean surface O₃ for the year 2025. The fractional contribution of natural O₃ will be pushed back even farther in favor of industrial O₃ as compared to 1993 (Table 5 and Plate 7). The emission assumptions are based on the IPCC-recommended moderate growth scenario IS92a (section 2). In spite of the expected reduction of NO_x emissions in western Europe and North America (that currently dominate the global NO_x source), total NO_x emissions may increase by a third over the next 25 years. This will have important implications for air quality, in particular, at 15°–50°N latitude. Plate 4 shows that in 2025, not only may the 40 ppbv level at the surface be exceeded in most of the United States, Europe, and Asia, but the 50 ppbv level may also be exceeded. Moreover, large areas will suffer from reduced air quality as the 60 and 70 ppbv O₃ levels may be exceeded as well.

Obviously, the abatement of large-scale photochemical ozone pollution will be most effective if emission reductions are implemented on a hemispheric scale. Relatively rapid latitudinal dispersion affects background pollution concentrations so that critical levels are easily exceeded by superposed O₃ formation from local emissions. For example, despite emission reductions in western Europe and the United States, surface ozone levels in these regions will continue to grow because background ozone will increase on a hemispheric scale. This could, for example, pose a problem to the implementation and acceptance of air quality control measures since the efforts to reduce emissions may not lead to the expected O₃ concentration decrease in the regions where these efforts are made.

Since tropospheric O₃ is also a potent greenhouse gas, its increase contributes substantially to climate forcing. By applying the same IPCC IS92a emission scenarios for 1993 and 2025, Roelofs *et al.* [1998] calculate that pollutant O₃ currently contributes 0.42 W m⁻² to the global mean radiative forcing of climate and may contribute 0.73 W m⁻² in 2025. Note that for the preindustrial scenario, only natural emissions were considered in order to isolate the anthropogenic effect. This present-day radiative forcing of 0.42 W m⁻² is within the range of previous estimates (0.28–0.55 W m⁻²) [Hauglustaine *et al.*, 1994; Van Dorland *et al.*, 1997; Berntsen *et al.*, 1997; Haywood *et al.*, 1998]. This is about 25% of the forcing by CO₂, and our calculations suggest that this fraction will remain the same in

2025. Our 2025 calculations furthermore indicate that tropospheric O₃ formation will continue to be NO_x controlled, in agreement with Wang and Jacob [1998]. Therefore abatement of large-scale O₃ pollution needs to focus on NO_x. This constitutes a difficult problem because NO_x emissions not only scale with fossil energy use but also with combustion efficiency (i.e., combustion temperature), which are both expected to increase in future. Hence it continues to be an important technological and societal challenge to reduce these emissions.

8. Conclusions

We presented model simulations of tropospheric ozone for the 1979–1993 period based on 15 years of ECMWF meteorological reanalyses [Gibson *et al.*, 1997] and a new emission data set that accounts for the temporal development of anthropogenic activities (Van Aardenne *et al.*, submitted manuscript, 1999). Comparison of the results with ozone observations suggests that the model represents the main processes that control tropospheric ozone. The model indicates that although STE provides an important ozone flux to the troposphere, in situ photochemistry largely controls the abundance and distribution of O₃ in the part of the troposphere that can be characterized as radiatively and chemically active. In the Northern Hemisphere the levels as well as the seasonal cycle of surface O₃ are dominated by photochemical processes. In the Southern Hemisphere, surface O₃ is also largely controlled by photochemistry; however, STE contributes more strongly to the seasonal cycle at background locations. The reason is that photochemistry in the Northern Hemisphere is more strongly enhanced by man-made emissions of O₃ precursors, in particular, of NO_x.

Source attribution of tropospheric O₃ by simulations of marked tracers shows that STE significantly contributes to those parts of the troposphere where radiative and thus photochemical processes are quiescent. Whenever such air masses are transported to regions with higher radiation intensities, photochemistry takes control of ozone. Hence the lifetime of STE-derived O₃ in the troposphere is largely controlled by transport. Ozone that has been photochemically produced in the troposphere also contributes significantly to the O₃ budget of the lowermost stratosphere, especially in summer. For example, in the summertime lowermost stratosphere (200 hPa) at lower midlatitudes, tropospheric O₃ exceeds stratospheric O₃ as a consequence of the higher tropopause and cross-tropopause transports.

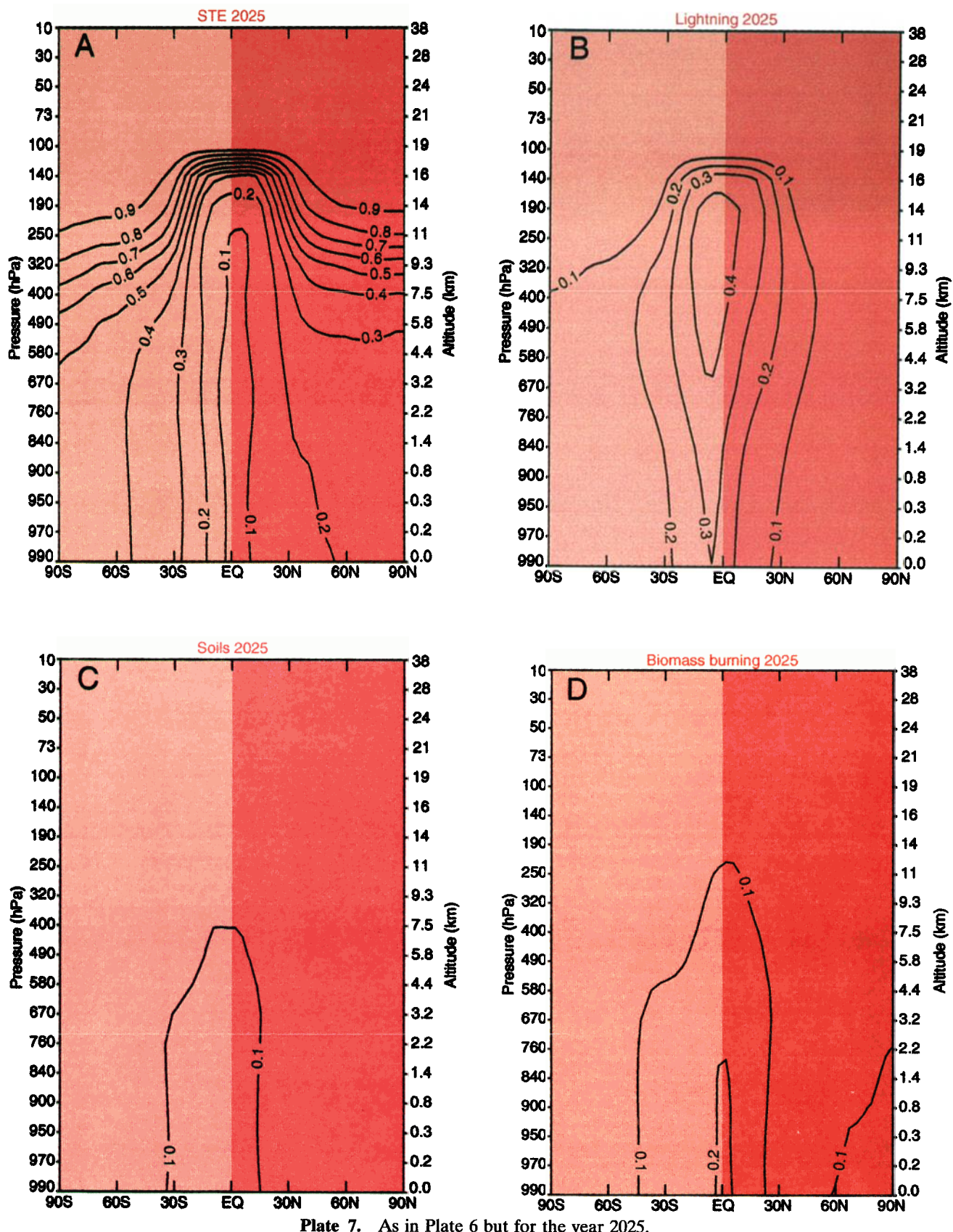


Plate 7. As in Plate 6 but for the year 2025.

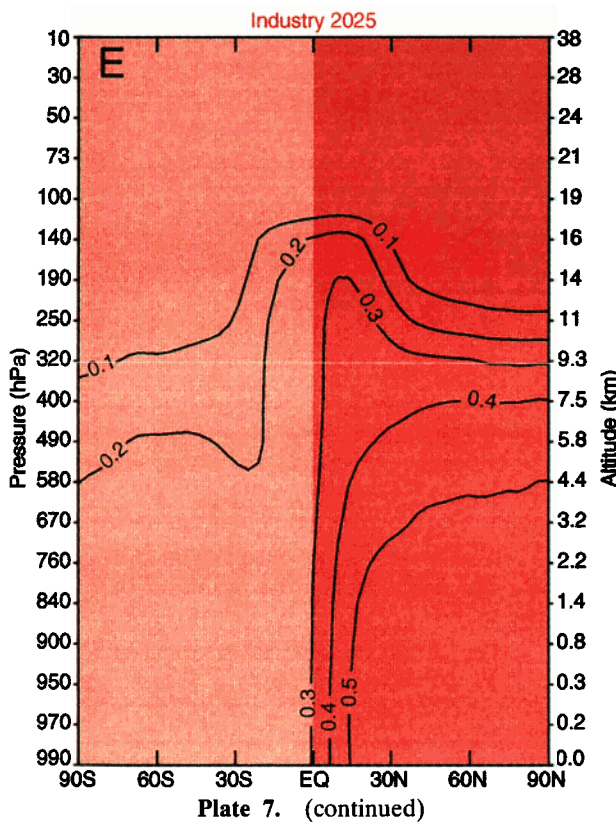


Plate 7. (continued)

Our O_3 source analysis indicates that although man-made pollution sources strongly contribute to tropospheric O_3 in the Northern Hemisphere, natural emissions are also important, especially lightning NO_x production at low latitudes. Considering the uncertainties associated with lightning emission estimates, however, our source attribution of tropospheric O_3 in the tropics is probably less accurate. A more detailed comparison of model results with measurements in the tropics, in particular in Africa, is presented by Marufu *et al.* [2000]. Furthermore, soil emissions of NO_x may have strongly increased as a result of fertilizer use, which can be significant for O_3 formation in areas that are still relatively unaffected by industrial emissions. However, the natural and anthropogenic soil emission estimates are also uncertain and need further investigation.

Our ozone source analysis suggests that photochemical O_3 formation from biomass burning emissions is less important than is indicated by previous studies. The main reason is that we quantify O_3 formation through the catalytic action of NO_x . Biomass burning emissions in the tropics and subtropics are relatively low in NO_x (e.g., compared to fossil fuel combustion). Moreover, much of the biomass burning NO_x is removed on a relatively small scale, whereas important O_3 formation in the burning plumes takes place on a large scale. It appears that natural NO_x (mainly from lightning) mixes with the burning effluents and strongly enhances O_3 formation. In our analysis we call this "natural ozone," although the CO and hydrocarbons oxidized in the process may be anthropogenic. The importance of this process is underscored by a simulation of preindustrial O_3 in which lightning NO_x is an even stronger contributor to tropospheric O_3 . We further note that Marufu *et al.* [2000] compared our marked NO_x approach with calcula-

tions in which all emissions per source category were switched on and off, and very similar results were obtained with both methods.

Finally, we simulated tropospheric ozone for the year 2025 on the basis of the IPCC-recommended IS92a moderate growth emission scenario. Our source analysis indicates that surface ozone will increase particularly strongly at subtropical northern latitudes because of NO_x emissions from fossil fuel use. Although it is precarious to predict future industrial growth, it seems very likely that the use of combustion technology and thus of NO_x emissions will increase in the developing world. Although NO_x emissions may even decrease in western Europe and North America in the next decades, tropospheric ozone will increase on a hemispheric scale. We calculate that as a result, critical O_3 levels will be substantially exceeded in the southern parts of the United States, Europe, and Asia.

Acknowledgments. F.J.D. was supported by the European Union through grant ENV4-CT97-0483 as part of the Environment Programme. We thank Rinus Scheele and Peter van Velthoven (KNMI) for the preprocessing of ECMWF data and Ad Jeukens (KNMI) and Maarten Krol (IMAU) for their contributions to model development. We thank E. Brunke, S. Oltmans, H. Scheel, J. Stähelin, and other colleagues that have contributed ozone measurement data through NOAA/CMDL and the World Ozone Data Center of the WMO.

References

- Akimoto, H., et al., Long-range transport of ozone in the East Asian Pacific rim region, *J. Geophys. Res.*, 101, 1999–2010, 1996.
- Alexis, N., S. M. Tarlo, and F. Silverman, Effects of ozone in human studies, in *Environmental Oxidants*, edited by J. O. Nriagu and M. S. Simmons, pp. 319–350, John Wiley, New York, 1994.
- Amann, M., M. Baldi, C. Heynes, Z. Klimont, and W. Schöpp, Integrated assessment of emission control scenarios, including the impact of tropospheric ozone, *Water Air Soil Pollut.*, 85, 2595–2600, 1995.
- Appenzeller, C., and J. R. Holton, Tracer lamination in the stratosphere: A global climatology, *J. Geophys. Res.*, 103, 13,555–13,569, 1997.
- Appenzeller, C., J. R. Holton, and K. H. Rosenlof, Seasonal variation of mass transport across the tropopause, *J. Geophys. Res.*, 101, 15,071–15,078, 1996.
- Berntsen, T. K., and I. S. A. Isaksen, A global three-dimensional chemical transport model for the troposphere, 1, Model description and CO and ozone results, *J. Geophys. Res.*, 102, 21,239–21,280, 1997.
- Berntsen, T. K., I. S. A. Isaksen, G. Myhre, J. S. Fuglestvedt, F. Stordal, T. A. Larsen, R. S. Freckleton, and K. P. Shine, Effects of anthropogenic emissions on tropospheric ozone and its radiative forcing, *J. Geophys. Res.*, 102, 28,101–28,126, 1997.
- Brewer, A. W., Evidence of a world circulation provided by the measurements of helium and water vapour distribution in the stratosphere, *Q. J. R. Meteorol. Soc.*, 75, 351–363, 1949.
- Carbon Dioxide Information Analysis Center (CDIAC), *Northern Hemisphere Biome and Process Specific Forest Areas and Gross Merchantable Volumes: 1890–1990*, edited by A. L. Brenkert, Oak Ridge Nat. Lab., Oak Ridge, Tenn., 1997.
- Chameides, W. L., and J. C. G. Walker, A time-dependent photochemical model for ozone near the ground, *J. Geophys. Res.*, 81, 413–420, 1976.
- Chameides, W. L., et al., Ozone precursor relationships in the ambient atmosphere, *J. Geophys. Res.*, 97, 6037–6055, 1992.
- Chameides, W. L., P. S. Kasibhatla, J. Yienger, J. Richardson, and C. S. Kiang, Growth of continental-scale metro-agro-plexes, regional ozone pollution, and world food production, *Science*, 264, 74–76, 1994.
- Charney, J. G., and P. G. Drazin, Propagation of planetary-scale disturbances from the lower into the upper atmosphere, *J. Geophys. Res.*, 66, 83–103, 1961.

- Chatfield, R., and H. Harrison, Ozone in the remote troposphere, mixing versus photochemistry, *J. Geophys. Res.*, **81**, 421–423, 1976.
- Crutzen, P. J., A discussion of the chemistry of some minor constituents in the stratosphere and troposphere, *Pure Appl. Geophys.*, **106–108**, 1385–1399, 1973.
- Crutzen, P. J., Photochemical reactions initiated by and influencing ozone in unpolluted tropospheric air, *Tellus*, **26**, 47–57, 1974.
- Crutzen, P. J., Tropospheric ozone: A review, in *Tropospheric Ozone: Regional and Global Scale Interactions*, edited by I. S. A. Isaksen, pp. 3–32, D. Reidel., Norwell-Mass., 1988.
- Crutzen, P. J., and P. H. Zimmermann, The changing chemistry of the troposphere, *Tellus, Ser. AB*, **43**, 136–151, 1991.
- Crutzen, P. J., M. Lawrence, and U. Poschl, On the background photochemistry of tropospheric ozone, *Tellus, Ser. AB*, **51**, 123–146, 1999.
- Danielsen, E. F., Stratospheric-tropospheric exchange based on radioactivity, ozone and potential vorticity, *J. Atmos. Sci.*, **25**, 502–518, 1968.
- Davies, T. D., and E. Schuepbach, Episodes of high ozone concentrations at the Earth's surface resulting from transport down from the upper troposphere/lower stratosphere: A review and case studies, *Atmos. Environ.*, **28**, 53–68, 1994.
- Delany, A. C., P. Haagenson, S. Walters, A. F. Wartburg, and P. J. Crutzen, Photochemically produced ozone in the emissions of large-scale tropical vegetation fires, *J. Geophys. Res.*, **90**, 2425–2429, 1985.
- Dentener, F. J., and P. J. Crutzen, Reaction of N_2O_5 on tropospheric aerosols: Impact on the global distributions of NO_x , O_3 , and OH, *J. Geophys. Res.*, **98**, 7149–7163, 1993.
- Dentener, F. J., J. Feichter, and A. Jeukens, Simulation of transport of Rn^{222} using on-line and off-line global models at different horizontal resolutions: A detailed comparison with measurements, *Tellus, Ser. B*, **51**, 573–602, 1999.
- Derwent, R. G., A. E. J. Eggleton, M. L. Williams, and C. A. Bell, Elevated ozone levels from natural sources, *Atmos. Environ.*, **12**, 2173–2177, 1978.
- Diab, R. D., et al., Vertical ozone distribution over southern Africa and adjacent oceans during SAFARI-92, *J. Geophys. Res.*, **101**, 23,823–23,833, 1996.
- Dobson, G. B. M., Origin and distribution of polyatomic molecules in the atmosphere, *Proc. R. Soc. London, Ser. A.*, **236**, 187–193, 1956.
- Dütsch, H. U., Photochemistry of atmospheric ozone, *Adv. Geophys.*, **15**, 219–322, 1971.
- Elbern, H., J. Kowal, R. Sladkovic, and A. Ebel, Deep stratospheric intrusions: A statistical assessment with model guided analysis, *Atmos. Environ.*, **31**, 3207–3226, 1997.
- Etheridge, D. M., L. P. Steele, R. J. Francey, and R. L. Langenfels, Atmospheric methane between 1000 A.D. and present: Evidence of anthropogenic emissions and climate variability, *J. Geophys. Res.*, **103**, 15,979–15,993, 1998.
- Fabian, P., and P. G. Pruchniewicz, Meridional distribution of ozone in the troposphere and its seasonal variations, *J. Geophys. Res.*, **82**, 2063–2073, 1977.
- Fahey, D. W., et al., Polar ozone, Polar ozone, in *Scientific Assessment of Ozone Depletion: 1994, Rep. 47*, pp. 3.1–3.53, World Meteorol. Org., Geneva, 1995.
- Fiore, A. M., D. J. Jacob, J. A. Logan, and Y. H. Yin, Long-term trends in ground level ozone over the contiguous United States, 1980–1995, *J. Geophys. Res.*, **103**, 1471–1480, 1998.
- Fishman, J., S. Solomon, and P. J. Crutzen, Observational and theoretical evidence in support of a significant in-situ photochemical source of tropospheric ozone, *Tellus*, **31**, 432–446, 1979.
- Fishman, J., C. E. Watson, J. C. Larson, and J. A. Logan, Distribution of tropospheric ozone determined from satellite data, *J. Geophys. Res.*, **95**, 3599–3617, 1990.
- Follows, M. J., and J. F. Austin, A zonal average model of the stratospheric contributions to the tropospheric ozone budget, *J. Geophys. Res.*, **97**, 18,047–18,060, 1992.
- Fortuin, P., and H. Kelder, An ozone climatology based on ozone sonde and satellite measurements, *J. Geophys. Res.*, **103**, 31,709–31,734, 1998.
- Ganzeveld, L. N., G.-J. Roelofs, and J. Lelieveld, A dry deposition parameterization for sulfur oxides in a chemistry and general circulation model, *J. Geophys. Res.*, **103**, 5679–5694, 1998.
- Gettelman, A., J. R. Holton, and K. H. Rosenlof, Mass fluxes of O_3 , CH_4 , N_2O , and CF_2Cl_2 in the lower stratosphere calculated from observational data, *J. Geophys. Res.*, **102**, 19,149–19,159, 1997.
- Gibson, R., P. Kallberg, and S. Uppala, The ECMWF re-analysis (ERA) project, *ECMWF Newslett.*, **73**, 7–11, 1997.
- Guille, W., Y. J. Balkanski, M. Schulz, F. Dulac, and P. Monfray, Wet deposition in a global size-dependent aerosol transport model, 1, Comparison of a 1 year ^{210}Pb simulation with ground measurements, *J. Geophys. Res.*, **103**, 11,429–11,445, 1998.
- Guenther, A., et al., A global model of natural volatile organic compound emissions, *J. Geophys. Res.*, **100**, 8873–8892, 1995.
- Haagen-Smit, A. J., and M. M. Fox, Ozone formation in photochemical oxidation of organic substances, *Ind. Eng. Chem. Res.*, **48**, 1484–1487, 1956.
- Haan, D., P. Martinerie, and D. Raynaud, Ice core data of atmospheric carbon monoxide over Antarctica and Greenland during the last 200 years, *Geophys. Res. Lett.*, **23**, 2235–2238, 1996.
- Harris, N. R. P., et al., Ozone measurements, in *Scientific Assessment of Ozone Depletion: 1994, Rep. 37*, pp. 1.1–1.54, World Meteorol. Org., Geneva, 1995.
- Hauglustaine, D. A., C. Granier, G. P. Brasseur, and G. Mégie, The importance of atmospheric chemistry in the calculation of radiative forcing on the climate system, *J. Geophys. Res.*, **99**, 1173–1186, 1994.
- Hauglustaine, D. A., G. P. Brasseur, S. Walters, P. J. Rasch, J.-F. Müller, L. K. Emmons, and M. A. Carroll, MOZART, a global chemical transport model for ozone and related chemical tracers, 2, Model results and evaluation, *J. Geophys. Res.*, **103**, 28,291–28,335, 1998.
- Haynes, P. H., C. J. Marks, M. E. McIntyre, T. G. Shepherd, and K. P. Shine, On the “downward control” of extratropical diabatic circulations by eddy-induced mean zonal forces, *J. Atmos. Sci.*, **48**, 651–687, 1991.
- Haywood, J. M., M. D. Schwartzkopf, and V. Ramaswamy, Estimates of radiative forcing due to modeled increases in tropospheric ozone, *J. Geophys. Res.*, **103**, 16,999–17,007, 1998.
- Hertel, O., R. Berkowicz, J. Christensen, and Ø. Hov, Test of two numerical schemes for use in atmospheric transport-chemistry models, *Atmos. Environ., Part A*, **27**, 2591–2611, 1993.
- Holdsworth, G., K. Higuchi, G. A. Zielinski, P. A. Mayewski, M. Wahln, B. Deck, P. Chylek, B. Johnson, and P. Damiano, Historical biomass burning: Late 19th century pioneer agriculture revolution in Northern Hemisphere ice core data and its atmospheric interpretation, *J. Geophys. Res.*, **101**, 23,317–23,334, 1996.
- Holton, J. R., P. H. Haynes, M. E. McIntyre, A. R. Douglass, R. B. Rood, and L. Pfister, Stratosphere-troposphere exchange, *Rev. Geophys.*, **33**, 403–439, 1995.
- Houweling, S., F. J. Dentener, and J. Lelieveld, The impact of non-methane hydrocarbon compounds on tropospheric photochemistry, *J. Geophys. Res.*, **103**, 10,673–10,696, 1998.
- Janach, W. E., Surface ozone: Trend details, seasonal variations, and interpretation, *J. Geophys. Res.*, **94**, 18,289–18,295, 1989.
- Jacob, D. J., J. A. Logan, G. M. Gardner, R. M. Yevich, C. M. Psivakovskiy, and S. C. Wofsy, Factors regulating ozone over the United States and its export to the global atmosphere, *J. Geophys. Res.*, **98**, 14,817–14,826, 1993.
- Johnston, H., and D. Kinnison, Methane photooxidation in the atmosphere: Contrast between two methods of analysis, *J. Geophys. Res.*, **103**, 21,967–21,984, 1998.
- Jones, R. L., et al., Tropical and midlatitude ozone, in *Scientific Assessment of Ozone Depletion: 1994, Rep. 37*, pp. 4.1–4.38, World Meteorol. Org., Geneva, 1995.
- Junge, C. E., Global ozone budget and exchange between stratosphere and troposphere, *Tellus*, **14**, 363–377, 1962.
- Kentarchos, A. S., G.-J. Roelofs, and J. Lelieveld, Model study of a stratospheric intrusion event at lower midlatitudes associated with the development of a cut-off low, *J. Geophys. Res.*, **104**, 1717–1727, 1999.
- Kley, D., H. Geiss, and V. A. Mohnen, Tropospheric ozone at elevated sites and precursor emissions in the United States and Europe, *Atmos. Environ.*, **28**, 149–158, 1994.
- Krol, M., and M. van Weele, Implication of variation of photodissociation rates for global atmospheric chemistry, *Atmos. Environ.*, **31**, 1257–1273, 1997.
- Landgraf, J., and P. J. Crutzen, An efficient method for online calculations of photolysis and heating rates, *J. Atmos. Sci.*, **55**, 863–878, 1998.
- Leighton, P. A., *Photochemistry of Air Pollution*, Academic, San Diego, Calif., 1961.
- Lelieveld, J., and R. van Dorland, Model simulations of ozone chem-

- istry changes in the troposphere and consequent radiative forcings of climate during industrialization, in *Atmospheric Ozone As a Climate Gas, NATO ASI Ser., Ser. 1*, vol. 32, edited by W.-C. Wang and I. S. A. Isaksen, pp. 227–258, Springer-Verlag, New York, 1995.
- Lelieveld, J., F. Arnold, B. Bregman, V. Burger, P. Crutzen, H. Fischer, P. Siegmund, P. van Velthoven, and A. Waibel, Chemical perturbation of the lowermost stratosphere through exchange with the troposphere, *Geophys. Res. Lett.*, **24**, 603–606, 1997.
- Lelieveld, J., P. J. Crutzen, and F. J. Dentener, Changing concentration, lifetime and climate forcing of atmospheric methane, *Tellus, Ser. B*, **50**, 128–150, 1998.
- Lelieveld, J., A. M. Thompson, R. D. Diab, Ø. Hov, D. Kley, J. A. Logan, O. J. Nielsen, W. R. Stockwell, and X. Zhou, Tropospheric ozone and related processes, in *Scientific Assessment of Ozone Depletion 1998, Rep. 44*, pp. 8.1–8.42, World Meteorol. Org., Geneva, 1999.
- Levy, H., II, Normal atmosphere. Large radical and formaldehyde concentrations predicted, *Science*, **173**, 141–143, 1971.
- Levy, H., II, J. D. Mahlman, W. L. Moxim, and S. C. Liu, Tropospheric ozone: The role of transport, *J. Geophys. Res.*, **90**, 3753–3771, 1985.
- Levy, H., II, P. S. Kasibhatla, W. J. Moxim, A. A. Klonecki, A. I. Hirsch, S. J. Oltmans, and W. L. Chameides, The global impact of human activity on tropospheric ozone, *Geophys. Res. Lett.*, **24**, 791–794, 1997.
- Logan, J. A., Tropospheric ozone: Seasonal behavior, trends, and anthropogenic influence, *J. Geophys. Res.*, **90**, 10,463–10,482, 1985.
- Logan, J. A., Trends in the vertical distribution of ozone: An analysis of ozone sonde data, *J. Geophys. Res.*, **99**, 25,553–25,585, 1994.
- London, J., and S. C. Liu, Long-term tropospheric and lower stratospheric ozone variations from ozone sonde observations, *J. Atmos. Terr. Phys.*, **5**, 599–625, 1992.
- Louis, J. F., A parametric model of vertical eddy fluxes in the atmosphere, *Boundary Layer Meteorol.*, **17**, 187–202, 1979.
- Mahlman, J. D., Long-term dependence of surface fallout fluctuations upon tropopause-level cyclogenesis, *Arch. Meteorol. Geophys. Bioklimatol. Ser. A*, **18**, 299–311, 1969.
- Marufu, L., F. J. Dentener, J. Lelieveld, M. O. Andreae, and G. Helas, Photochemistry of the African troposphere: The influence of biomass burning emissions, *J. Geophys. Res.*, in press, 2000.
- McPeters, R. D., et al., *Nimbus-7 Total Ozone Mapping Spectrometer (TOMS) Data Products User's Guide*, NASA Ref. Publ., 1384, 1996.
- Muller, J.-F., and G. P. Brasseur, IMAGES: A three-dimensional chemical transport model of the global troposphere, *J. Geophys. Res.*, **100**, 16,445–16,490, 1995.
- National Research Council, *Rethinking the Ozone Problem in Urban and Regional Air Pollution*, Natl. Acad., Washington, D.C., 1991.
- Olivier, J., et al., *Description of EDGAR Version 2.0.. RIVM Rep. 771060002*, Rijksinst. voor Volksgezondheid en Milieu, Bilthoven, Netherlands, 1996.
- Oltmans, S. J., and H. Levy II, Surface ozone measurements from a global network, *Atmos. Environ.*, **28**, 9–24, 1994.
- Oltmans, S. J., D. J. Hofmann, J. A. Lathrop, J. M. Harris, W. D. Komhyr, and D. Kuniyuki, Tropospheric ozone during Mauna Loa Observatory Experiment 2 compared to long-term measurements from surface and ozone sonde observations, *J. Geophys. Res.*, **101**, 14,569–14,580, 1996.
- Oltmans, S. J., et al., Trends of ozone in the troposphere, *Geophys. Res. Lett.*, **25**, 139–142, 1998.
- Penkett, S. A., and K. A. Brice, The spring maximum of photo-oxidants in the Northern Hemisphere troposphere, *Nature*, **319**, 655–657, 1986.
- Penkett, S. A., C. E. Reeves, B. J. Bandy, J. M. Kent, and H. R. Richer, Comparison of calculated and measured peroxide data collected in marine air to investigate prominent features of the annual cycle of ozone in the troposphere, *J. Geophys. Res.*, **103**, 13,377–13,388, 1998.
- Pickering, K. E., et al., Convective transport of biomass burning emissions over Brazil during TRACE-A, *J. Geophys. Res.*, **101**, 23,993–24,012, 1996.
- Reed, R. J., A study of a characteristic type of upper-level frontogenesis, *J. Meteorol.*, **12**, 226–237, 1955.
- Regener, V. H., Vertical flux of atmospheric ozone, *J. Geophys. Res.*, **62**, 221–228, 1957.
- Reiter, E. R., Stratosphere-troposphere exchange processes, *Rev. Geophys.*, **13**, 459–474, 1975.
- Reiter, E. R., On the mean daily and seasonal variations of the vertical ozone profiles in the lower troposphere, *Atmos. Environ., Part A*, **25**, 1751–1757, 1991.
- Roelofs, G.-J., and J. Lelieveld, Distribution and budget of O₃ in the troposphere calculated with a chemistry-general circulation model, *J. Geophys. Res.*, **100**, 20,983–20,998, 1995.
- Roelofs, G.-J., and J. Lelieveld, Model study of the influence of cross-tropopause O₃ transports on tropospheric O₃ levels, *Tellus, Ser. B*, **49**, 38–55, 1997.
- Roelofs, G.-J., J. Lelieveld, and R. van Dorland, A three-dimensional chemistry/general circulation model simulation of anthropogenically derived ozone in the troposphere and its radiative climate forcing, *J. Geophys. Res.*, **102**, 23,389–23,401, 1997.
- Roelofs, G.-J., J. Lelieveld, and J. Feichter, Model simulations of the changing distribution of ozone and its radiative forcing of climate: Past, present and future, *Rep. 283*, Max-Planck-Instit. for Meteorol., Hamburg, Germany, 1998.
- Russel, G., and J. Lerner, A new finite difference scheme for the tracer transport equation, *J. Appl. Meteorol.*, **20**, 1483–1498, 1981.
- Russell, J. M., III, et al., The Halogen Occultation Experiment, *J. Geophys. Res.*, **98**, 10,777–10,797, 1993.
- Sandroni, S., D. Anfossi, and S. Viarengo, Surface ozone levels at the end of the nineteenth century in South America, *J. Geophys. Res.*, **97**, 2535–2539, 1992.
- Sillman, S., J. A. Logan, and S. C. Wofsy, The sensitivity of ozone to nitrogen oxides and hydrocarbons in regional ozone episodes, *J. Geophys. Res.*, **95**, 1837–1851, 1990.
- Staehelin, J., J. Thudium, R. Buehler, A. Volz-Thomas, and W. Grauber, Trends in surface ozone concentrations at Arosa (Switzerland), *Atmos. Environ.*, **28**, 75–87, 1994.
- Thompson, A. M., K. E. Pickering, D. P. McNamara, M. R. Schoeberl, R. D. Hudson, J. H. Kim, E. V. Browell, V. W. J. H. Kirchhoff, and D. Nganga, Where did tropospheric ozone over southern Africa and the tropical Atlantic come from in October 1992? Insights from TOMS, GTE TRACE A, and SAFARI 1992, *J. Geophys. Res.*, **101**, 24,251–24,278, 1996.
- Tie, X., and P. Hess, Ozone mass exchange between the stratosphere and troposphere for background and volcanic sulfate aerosol conditions, *J. Geophys. Res.*, **102**, 25,478–25,500, 1997.
- Tiedtke, M., A comprehensive mass-flux scheme for cumulus parameterization in large-scale models, *Mon. Weather Rev.*, **117**, 1779–1800, 1989.
- Tsutsumi, Y., Y. Igarashi, Y. Zaizen, and Y. Makino, Case studies of tropospheric ozone events observed at the summit of Mount Fuji, *J. Geophys. Res.*, **103**, 16,935–16,951, 1998.
- Tuck, A. F., et al., Strat-trop exchange, in *Atmospheric Ozone 1985, Rep. 16*, pp. 151–240, World Meteorol. Org., Geneva, 1985.
- U.S. Environmental Protection Agency (EPA), National air pollution emissions trends, 1900–1995, *EPA-454/R-96-007*, Research Triangle Park, N. C., 1996.
- Van Dorland, R., F. J. Dentener, and J. Lelieveld, Radiative forcing due to tropospheric ozone and sulfate aerosol, *J. Geophys. Res.*, **102**, 28,079–28,100, 1997.
- Volz, A., and D. Kley, Ozone measurements made in the 19th century: An evaluation of Montsouris series, *Nature*, **332**, 240–242, 1988.
- Volz-Thomas, A., Trends in photo-oxidant concentrations, in *Proceedings of EUROTAC Symposium '92*, edited by P. M. Borrell, pp. 59–64, SPB Acad., The Hague, Netherlands, 1993.
- Wang, Y., and D. J. Jacob, Anthropogenic forcing on tropospheric ozone and OH since preindustrial times, *J. Geophys. Res.*, **103**, 31,123–31,135, 1998.
- Wang, Y., D. J. Jacob, and J. A. Logan, Global simulation of tropospheric O₃-NO_x-hydrocarbon chemistry, 2, Model evaluation and global ozone budget, *J. Geophys. Res.*, **103**, 10,727–10,755, 1998.
- F. J. Dentener and J. Lelieveld, Institute for Marine and Atmospheric Research, Utrecht University, Princetonplein 5, 3584 CC Utrecht, Netherlands (j.lelieveld@phys.uu.nl)

(Received July 23, 1999; revised September 22, 1999; accepted September 27, 1999.)